JOURNAL OF VIROLOGY, July 2002, p. 6618–6635 Vol. 76, No. 13
0022-538X/02/$04.00+0 DOI: 10.1128/JVI.76.13.6618–6635.2002

Critical Role for Glial Cells in the Propagation and Spread of Lymphocytic Choriomeningitis Virus in the Developing Rat Brain

Daniel J. Bonthius,[1,2,3]* Jolonda Mahoney,[1] Michael J. Buchmeier,[4] Bahri Karacay,[1] and Derek Taggard[5]

Departments of Pediatrics,[1] Neurology,[2] Anatomy & Cell Biology,[3] and Neurosurgery,[5] University of Iowa College of Medicine, Iowa City, Iowa 52242, and Department of Neuropharmacology, The Scripps Research Institute, La Jolla, California 92037[4]

Received 19 December 2001/Accepted 4 April 2002

Inoculation of the neonatal rat with lymphocytic choriomeningitis virus (LCMV) results in the selective infection of several neuronal populations and in focal pathological changes. However, the pathway by which LCMV reaches the susceptible neurons has not been described, and the nature and time course of the pathological changes induced by the infection are largely unknown. This study examined the sequential migration of LCMV in the developing rat brain and compared the pathological changes among infected brain regions. The results demonstrate that astrocytes and Bergmann glia cells are the first cells of the brain parenchyma infected with LCMV and that the virus spreads across the brain principally via contiguous glial cells. The virus then spreads from glial cells into neurons. However, not all neurons are susceptible to infection. LCMV infects neurons in only four specific brain regions: the cerebellum, olfactory bulb, dentate gyrus, and periventricular region. The virus is then cleared from glial cells but persists in neurons. LCMV induces markedly different pathological changes in each of the four infected regions. The cerebellum undergoes an acute and permanent destruction, while the olfactory bulb is acutely hypoplastic but recovers fully with age. Neurons of the dentate gyrus are unaffected in the acute phase but undergo a delayed-onset mortality. In contrast, the periventricular region has neither acute nor late-onset cell loss. Thus, LCMV infects four specific brain regions in the developing brain by spreading from glial cells to neurons and then induces substantially different pathological changes with diverse time courses in each of the four infected regions.

Lymphocytic choriomeningitis virus (LCMV) is a rodent-borne arenavirus and a prevalent human pathogen (11, 12, 29). Infection of the postnatal human with LCMV typically results in only a mild febrile illness, from which the patient recovers fully. In contrast, when the infection occurs during pregnancy, the fetal brain can be severely damaged. Microencephaly, chorioretinitis, hydrocephalus, and periventricular calcifications are frequently noted features (6, 18, 46). These neuropathological changes lead to mental retardation, impaired coordination, spasticity, blindness, and epilepsy in children with congenital LCMV infection (5, 7, 46). The pathogenic mechanisms underlying LCMV-induced injury of the fetal human brain are unknown.

Although the human fetal brain is vulnerable throughout gestation to the teratogenic effects of LCMV, many of the case reports of congenital LCMV infection describe infants who were infected during the third or late second trimester (21, 23, 42, 46). This is a period of rapid brain growth, referred to as the brain growth spurt (17), and is a time when many neuroteratogens exert adverse effects (9, 15). While all mammalian species have a brain growth spurt, the timing of this event, relative to birth, varies among the species. Relative to the human brain, the rat brain is immature at birth, and the brain growth spurt in the rat occurs during the first two postnatal weeks (16, 17). Therefore, an accurate model of human mid- or late-gestation LCMV infection requires infection of the rat during early postnatal life.

The neonatal rat inoculated with LCMV serves as an excellent model system for human congenital LCMV infection. LCMV infection in suckling rats induces microencephaly, retinitis, and the selective destruction of several brain regions (32, 34, 38). These neuropathologic changes manifest as permanent abnormalities of movement, coordination, vision, and behavior, reminiscent of human congenital LCMV infection (14, 30, 31).

In the neonatal rat brain, inoculation of LCMV induces a distinct pattern of infection in which specific neuronal populations are consistently infected, while others are spared (13, 34). This selectivity of infection likely underlies the focal pathological changes which follow. However, the susceptible neuronal populations are widely separated, and the pathway by which LCMV reaches these neurons has not been identified. Elucidation of this pathway is of substantial importance, not only for a better understanding of LCMV biology and teratogenesis, but because the cells utilized by LCMV in its sequential spread are sites to which therapeutic agents could be targeted to block the infection.

One goal of this study was to examine the sequential migration of LCMV in the developing brain to identify the pathway by which LCMV reaches susceptible neurons. The results demonstrate that glial cells are the initial target cells of LCMV within the brain parenchyma and that LCMV spreads across the brain and reaches susceptible neuronal populations via

* Corresponding author. Mailing address: Department of Pediatrics, Division of Child Neurology, 2504 JCP, University of Iowa Hospital and Clinics, 200 Hawkins Dr., Iowa City, IA 52242. Phone: (319) 356-7727. Fax: (319) 356-4855. E-mail: daniel-bonthius@uiowa.edu.

glial cells. Thus, glial cells play a major role in the pathogenesis of LCMV in the developing brain. A second goal was to examine the natural history of LCMV infection of the developing rat brain and the neuropathologic changes that accompany it. The results demonstrate that LCMV infects neurons in four discrete brain regions, each of which contains mitotically active neuronal precursors. The pathology induced by LCMV in these four regions differs markedly, not only in time course and severity, but also in the type of pathology induced and in the capacity for recovery. Thus, the teratogenic mechanisms of LCMV within the developing brain vary from one infected region to another. The pathological changes observed in neonatal rats inoculated with LCMV closely mimic the neuropathology observed in humans with congenital LCMV infection.

MATERIALS AND METHODS

Animals. Pregnant Lewis rats at midgestation were obtained from Harlan Sprague-Dawley (Indianapolis, Ind.) and maintained in viral containment quarters at the University of Iowa Animal Care Facility. The rats were observed every 24 h to establish the time of birth of their litters. Day of birth was defined as postnatal day 0 (PD0) and was the 24-h period ending at 1700 h.

Virus. The neurotropic Armstrong-4 strain of LCMV was used throughout this study (38, 45). Virus stock was prepared in BHK-21 cells (multiplicity of infection [MOI], 0.1) harvested 48 h postinfection and stored in 1-ml aliquots at −70°C. The stock had a titer of 2×10^8 PFU per ml.

Infections. On PD4, unanesthetized male and female pups were infected with LCMV in the right frontal cortex by a modification of a procedure described previously (4). A Hamilton syringe with a needle depth guard was used for the intracerebral injection of 1,000 PFU of LCMV in a volume of 10 μl of Dulbecco's modified Eagle's medium (DMEM). Uninfected control littermates received sham intracerebral injections of 10 μl of DMEM. Because rat pups excrete and secrete virus that can infect littermates, littermate controls were fostered to unexposed mothers with unexposed litters.

Perfusions, LCMV immunohistochemistry, and pathological analysis. The rats were killed by pentobarbital overdose at a series of ages postinoculation, including PD5,-6,-8,-10,-12,-15,-18,-25,-30,-49,-60,-90, and -120. Two rats were included at each time point except the PD30 and PD120 time points, which included nine rats. The rats were perfused via the left cardiac ventricle with 0.9% ice-cold saline followed by a buffered fixative consisting of 4% paraformaldehyde in 0.1 M sodium phosphate. The brains, including the olfactory bulbs, were removed and stored in 4% paraformaldehyde fixative overnight.

Two of the brains from each time point were chosen for immunohistochemical studies. These brains were placed in 30% sucrose in 0.1 M sodium phosphate at 4°C until they sank. The brainstem, with cerebellum attached, was dissected free of the forebrain via a cut between the superior and inferior colliculi. In some cases, the olfactory bulbs were left attached to the remainder of the forebrain, while in others, the olfactory bulbs were dissected away from the forebrain via a cut through the olfactory stalk.

Fifty-micrometer-thick sections were cut on a sliding microtome. Most of the forebrains were cut in the horizontal plane, while the hindbrains were cut in the sagittal plane. A few forebrains were cut in the parasagittal plane in order to include the olfactory bulb and attached cerebrum in a single section along the longitudinal axis of the forebrain. Olfactory bulbs that were dissected free of the remaining forebrains were cut in the coronal plane. All sections were saved, and a 1:10 series of sections were mounted on glass slides and Nissl stained with cresyl violet for detection of pathological changes. The remaining sections were stored in cryopreservative until used for immunohistochemistry.

Staining for LCMV antigen was performed on floating sections. The sections were first incubated with 3% hydrogen peroxide for 30 min, followed by goat serum blocking solution for 60 min, and then incubated with guinea pig polyclonal anti-LCMV antibody (4) (1:1,000) overnight at 4°C. Detection was performed with a biotinylated goat anti-guinea pig immunoglobulin secondary antibody (Jackson ImmunoResearch, West Grove, Pa.) followed by ABC Elite (Vector Laboratories, Burlingame, Calif.) and diaminobenzidine substrate. Phosphate-buffered saline (PBS) was used for all dilutions and rinses.

Some sections adjacent to those stained for LCMV were stained immunohistochemically for glial fibrillary acidic protein (GFAP) in order to identify astrocytes and Bergmann glia. The technique for the GFAP staining was identical to that used for LCMV staining except that the primary antibody was a polyclonal rabbit anti-rat GFAP antibody (Sigma, St. Louis, Mo.), and the secondary antibody was a biotinylated goat anti-rabbit immunoglobulin G (IgG) (Vector Laboratories, Burlingame, Calif.).

Neuronal counts. To determine the effect of LCMV infection on neuronal numbers, cell counts were performed. Neuronal counts were obtained on PD30 to determine the acute effects of infection and on PD120 to examine the long-term consequences. Seven infected and seven sham-infected rats were used at each time point. Neuronal counts were obtained from the olfactory bulb, hippocampal formation, and septum in order to demonstrate the differences in time course and severity of neuronal loss among the various infected regions.

The brains were postfixed in cold fixative for 2 to 3 months. The cerebellum and brain stem were dissected free of the forebrains. In order to ensure that sampling of the hippocampal formation and septum occurred at a uniform dorsal-ventral level in each animal, the forebrains were initially cut with an Oxford vibratome in sections of 200-μm thickness in the horizontal plane. The section of forebrain containing the interventricular foramen was collected. (This level corresponds to the horizontal plane approximately 5.6 mm ventral to the bregma [36] and is the region along the septotemporal axis where the hippocampal formation is most uniform in size and where the septum acquires a characteristic shape.) The thick sections were then dehydrated through a graded series of alcohols and embedded in JB4 (Polysciences, Inc.), a water-soluble plastic, between two pieces of Aclar. This configuration kept the sections flat in order to allow later sectioning in the horizontal plane. After the JB4 had solidified, each septum and left hippocampal formation was excised from the thick horizontal section and embedded in a Beem capsule containing JB4.

In order to quantify neurons from a uniform position within the olfactory bulbs, a 1-mm-thick coronal slice was taken from the midpoint of each oval-shaped left olfactory bulb (10). The cuts were made in the plane orthogonal to the longitudinal axis of each bulb. This position in the main olfactory bulb is rostral to the accessory olfactory bulb and is readily identifiable in all subjects (19, 36, 43). The slices were dehydrated and embedded in JB4 to allow sectioning in the coronal plane.

The cerebellar vermis was also embedded in JB4. For the uninfected animals, the cerebellum was first separated from the brainstem. However, because the cerebellum was so greatly atrophied in the infected animals, the brainstem was usually left attached to the cerebellum to facilitate orientation of the tissue. For all animals, the vermis was isolated from the cerebellar hemispheres, dehydrated, and embedded in JB4 with an orientation that allowed sectioning in the midsagittal plane.

The cerebellar vermis, hippocampal formation, olfactory bulb, and septum were then cut as 2-μm-thick sections on a Reichert-Jung Ultracut E ultramicrotome. The sections were stained with cresyl violet or with a combination of cresyl violet and saffranin O. Slides were coded and analyzed by investigators blind to the treatment groups.

Neuronal populations were quantified from single sections of the olfactory bulb, hippocampal formation, and septum of each animal. Cell counts were not performed in the cerebellum because the severe degree of pathology in that structure made it impossible to identify the cell types of many individual cells. The methods used for identifying and quantifying the various neuronal types of the olfactory bulb and hippocampus have been described in detail previously (8, 9, 10).

To determine the effect of LCMV infection on neuronal number within a specified nucleus of the septum, the neurons of the lateral septal nucleus were counted. The lateral septal nucleus consists of a relatively homogeneous population of medium-sized neurons and lies adjacent to the medial wall of the lateral ventricle. Its neuronal components can be readily distinguished from those of the medial septal nucleus (medially), triangular septal nucleus and subfornical organ (posteriorly), and the dorsal tenia tecta and infralimbic cortex (anteriorly) by differences in cell shape and size, staining characteristics, and packing densities (36).

Cells were counted with the point counting program of the Stereo Investigator software (MicroBrightField, Inc., Colchester, Vt.). Only cells with clearly discernible nuclear membranes were included in the counts.

The pyramidal cells of hippocampal fields CA1 and CA3, the granule cells of the dentate gyrus, and the mitral cells of the olfactory bulb were exhaustively counted in each section. For the olfactory granule cells and the neurons of the lateral septal nucleus, the large number of neurons constituting those populations made manual counts impractical. Thus, the number of neurons per section for these two neuronal populations was estimated through the use of the Stereo Investigator software by multiplying the cell layer area by the average density measurement, as previously described (8, 9, 10).

Virus quantification. A separate group of animals was used to quantify virus load in various cerebral and extracerebral tissues. On PD4, Lewis rat pups

received an injection of 1,000 PFU of LCMV in a volume of 10 μl of DMEM into the right cerebrum via a Hamilton syringe. All pups within a litter were injected and were immediately returned to their mothers. At a series of times postinoculation, including PD6,-8,-10,-12,-14,-16,-18,-25,-32,-38,-49, and -64, the rats were sacrificed for virus titer determinations. Four animals were included per time point. The rats were anesthetized with pentobarbital, and a 100-μl sample of blood was collected from the heart into a 1-ml syringe and then transferred into a sterile Eppendorf tube. The animals were then perfused with sterile ice-cold PBS and euthanized, and tissue samples were obtained.

Tissues sampled from the central nervous system included the right and left olfactory bulbs, right and left hippocampus (including dentate gyrus), right and left cerebral cortex, brain stem, cervical spinal cord, and cerebellar vermis. Because pilot data indicated that the dorsal and ventral regions of the cerebellar vermis may be differentially affected by LCMV infection, the vermis was bisected into dorsal and ventral halves, which were processed separately.

To determine the extent to which extracerebral tissues become infected in this model system, a set of tissue samples were obtained from the spleen, thymus, liver, kidney, and cervical muscle. Each of the sampled tissues was immediately frozen on powdered dry ice and then stored frozen at −70°C until processed for virus titer.

To determine the virus titer, each tissue sample was weighed and then homogenized in plaquing medium containing 2% fetal bovine serum, 1% penicillin/streptomycin, 1× L-glutamine, and 0.25 M HEPES in DMEM. Virus concentrations were determined by plaque assay on Vero cell monolayers, as previously described (44). Virus titers were recorded as $\log_{10}$ virus per gram of tissue (or per milliliter, in the case of blood).

Statistical analyses. For the virus titer data, one set of analyses was conducted on the regions of the central nervous system (CNS), and a separate set of analyses was conducted on the non-CNS regions. For both of the analyses, the distribution of the data was normalized through a logarithm transformation, log(value + 1), applied to the data prior to the analyses. The constant (+1) was added to each value in order to allow calculation of a geometric mean at each time point and for each tissue. (The virus titer was zero in multiple tissues at multiple time points, and geometric means cannot be calculated on data containing zeroes. Since most of the virus titers ranged in value from 10^3 to 10^9, the addition of the constant [+1] altered the values only trivially.)

The virus titer data on the regions of the CNS was analyzed by repeated-measures analysis of variance (ANOVA). The two factors in the analyses were age (the between-animal factor) and region (the within-animal repeated-measures factor). One statistical test compared virus titers within the right versus the left side of the cortex, hippocampus, and olfactory bulb at each age. The second test compared virus titers within the seven regions of the CNS at each age. Bonferroni's method was used to adjust for the number of statistical tests that were done for these sets of comparisons. A Bonferroni-adjusted P value of <0.05 was considered statistically significant.

For the non-CNS regions, the maximum titers for each region (regardless of the postnatal age at which the maximum occurred) were analyzed by one-way ANOVA. Post hoc individual comparisons among regions were conducted with Newman-Keuls analyses.

The number of neurons in each of the six cell populations examined (CA1 and CA3 pyramidal cells, dentate gyrus granule cells, olfactory mitral and granule cells, and cells of the lateral septal nucleus) were initially analyzed simultaneously with multivariate ANOVA incorporating all six dependent variables, with virus treatment and age at sacrifice as the between-group factors. Wilks' lambda was evaluated by F estimation. Follow-up analyses of significant group differences in total cell counts in the multivariate ANOVA included separate ANOVAs and Newman-Keuls tests for each dependent variable.

RESULTS

Throughout their lives, LCMV-infected animals remained healthy-appearing, well groomed, and active. At no time did the infected animals appear systemically ill. However, 10 to 12 days postinoculation, the infected animals developed hind limb hypotonia and global ataxia, which persisted throughout life.

Following intracerebral injection of LCMV on PD4, the first intracranial structures to show immunohistochemical evidence of infection were the leptomeninges, choroid plexus, and ependymal lining of the ventricular system. Each of these structures was heavily labeled as early as PD6 (postinoculation day 2). By PD8, the infection had spread into the brain parenchyma. However, as shown in Fig. 1 and 2, these initially infected parenchymal cells were exclusively glial cells and were not randomly or uniformly distributed throughout the brain but were located in semiconfluent patches immediately adjacent to the infected ependymal or meningeal surfaces. Glial cells within white matter tracts adjacent to the ventricular system, including the corpus callosum and fimbria-fornix, were particularly vulnerable to infection.

After PD8, the parenchymal infection had spread beyond glial cells to include neuronal populations. However, not all neurons were vulnerable to infection. On the contrary, despite widespread glial cell infection, neurons became infected in only four specific brain regions. These regions included the cerebellum, hippocampus, olfactory bulb, and the region surrounding the lateral ventricles. In each of these four regions, the pattern and evolution of LCMV infection were unique, as were the time course and nature of the infection-induced neuropathologic changes.

Cerebellum. (i) Topography of infection in the cerebellum. In the cerebellum, the first cells infected were the astrocytes adjacent to the fourth ventricle. As shown in Fig. 3, the principal mode of spread of the infection through the cerebellum was via contiguous astrocytes within the white matter. In this way, the infection spread from ventral to dorsal and from the proximal base of the cerebellar lobules to the distal tips. As the infection reached the cerebellar cortex, the virus spread from astrocytes to Bergmann glia but initially spared neurons.

A second, less prominent mode of viral spread through the cerebellum was in the opposite direction (Fig. 3). In this scenario, the infection spread from the leptomeninges to the Bergmann glia at the distal tips of the dorsal lobules. The infection then progressed inward toward the base of the lobules, again via adjacent astrocytes.

Figures 3 and 4 show that by PD10, these two modes of viral spread led to a nearly universal infection of cerebellar astrocytes and Bergmann glia. However, at this stage, the infection was virtually confined to glial cells. With the exception of an occasional labeled cerebellar granule cell, no cerebellar neurons contained viral antigen on PD10.

Figure 4 demonstrates the pattern by which the cellular site of LCMV infection within the cerebellum changed over time. After PD10, the infection spread rapidly from glial cells into neurons. By PD14, large quantities of viral antigen were present in Purkinje cells and in granule cells of both the external and internal granule cell layers.

Through PD18, viral antigen remained present in both glial cells and neurons. However, between PD18 and PD25, viral antigen was abruptly and totally cleared from glial cells, though neurons remained heavily labeled. Viral antigen remained detectable in neurons for several months but persisted for a greater duration in Purkinje cells than in granule cells. Viral antigen was last detectable in cerebellar granule cells on PD60 and in Purkinje cells on PD90.

(ii) Viral quantification in the cerebellum. Quantification of infectious virus confirmed the prominent ventral-to-dorsal spread of infection through the cerebellum. As shown in Fig. 5B, during the initial period of infection, the LCMV titer was several orders of magnitude greater in the ventral cerebellum than in the dorsal cerebellum. Virus titers equalized in the two

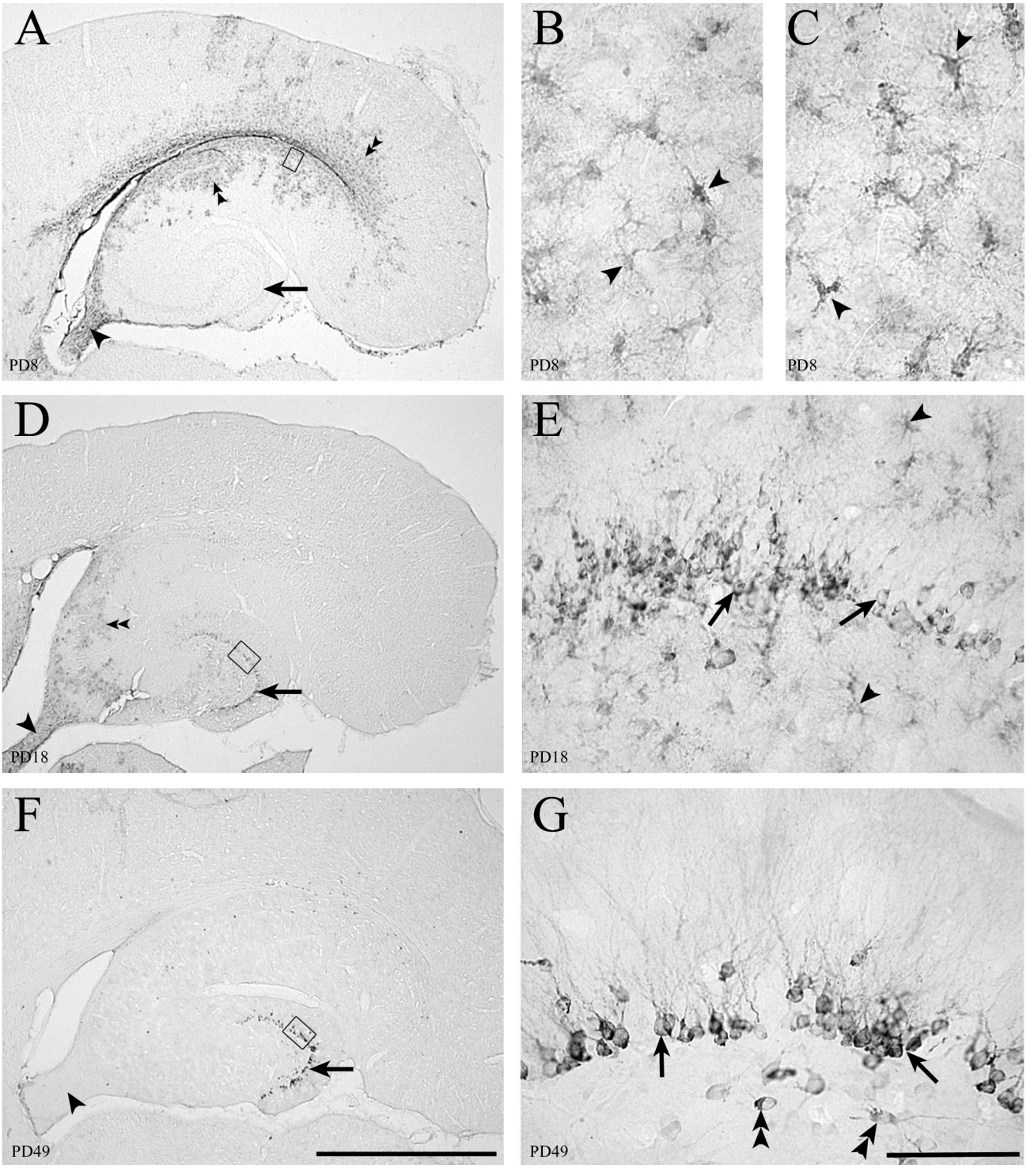

FIG. 1. Fifty-micrometer-thick sections through the hippocampal formation immunohistochemically stained for LCMV (panels A, B, D, E, F, and G) or GFAP (panel C). LCMV infection in the hippocampus initially involves astrocytes. The granule cells of the dentate gyrus become chronically infected. (A) Low-power image of hippocampal region at PD8 shows infection within the ependyma, parenchymal cells adjacent to the ependyma (double arrowheads), and fornix (arrowhead). The dentate gyrus (arrow) is not labeled. (B) Area beneath the ependyma, represented by the box in panel A, shows that the infected cells have the morphology of astrocytes (arrowheads). (C) A section adjacent to panel B immunohistochemically labeled for GFAP, a marker for astrocytes. The GFAP-positive cells in panel C have the same morphology as the LCMV-infected cells in panel B, indicating that the infected parenchymal cells on PD8 are astrocytes. (D) By PD18, infection in the hippocampal region is less intense but still present beneath the ependyma (double arrowheads) and in the fornix (arrowhead). The dentate gyrus stratum granulosum (arrow) now shows evidence of infection. (E) Higher magnification of box in panel D shows that granule cells of the dentate gyrus (arrows), and nearby astrocytes (arrowheads) are both infected with LCMV on PD18. (F) By PD49, infection has been cleared from the hippocampal region, including the fornix (arrowhead), except for granule cells of the dentate gyrus (arrow), where viral antigen persists. (G) Higher magnification of the box in panel F demonstrates that cell bodies and dendrites of dentate granule cells (arrows) and a few hilar neurons (double arrowheads) are still infected. The virus has been cleared from glial cells. Bars, 1 mm (A, D, and F); 20 μm (B and C); 100 μm (E and G).

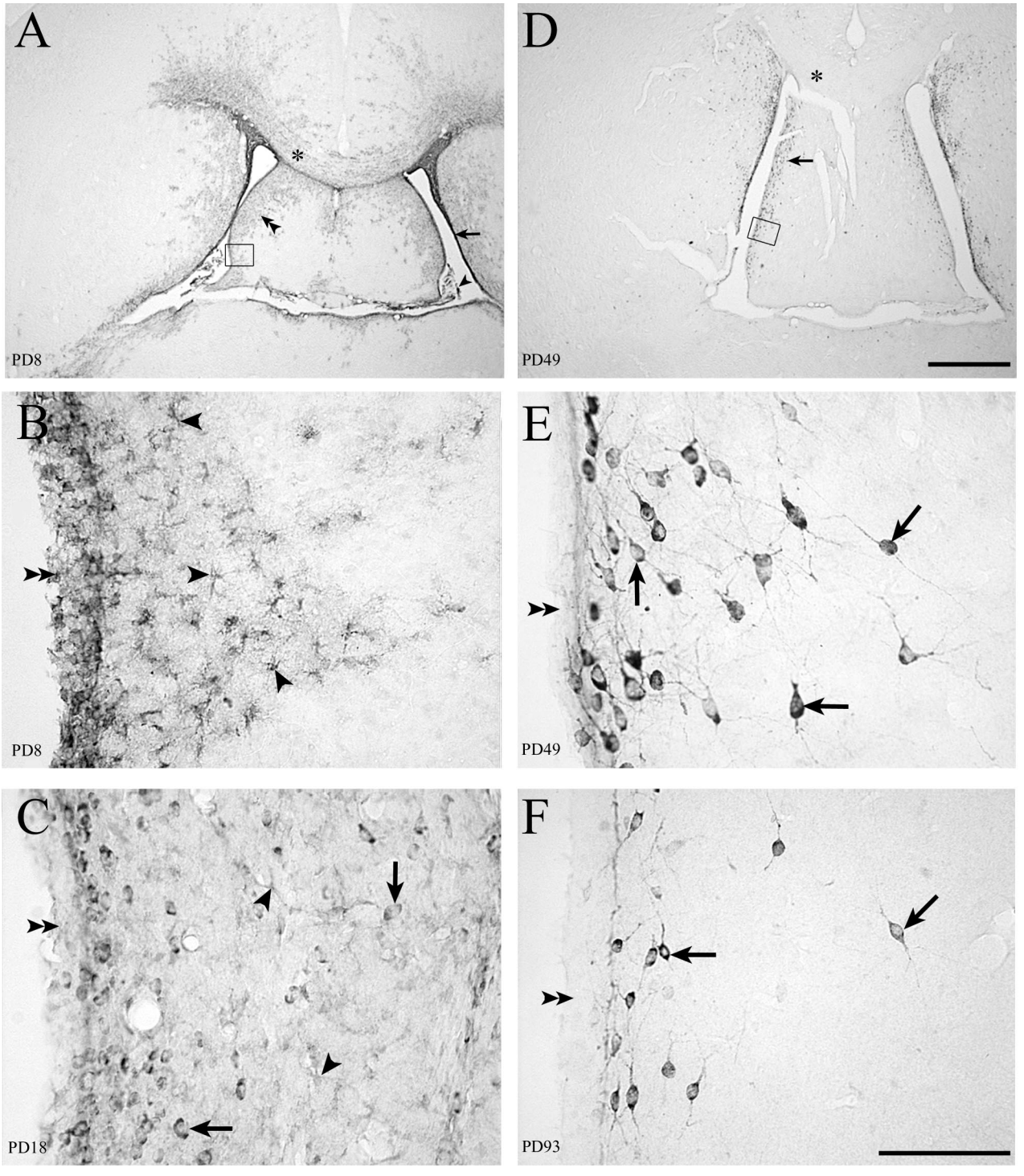

FIG. 2. Fifty-micrometer-thick sections through the septum immunohistochemically stained for LCMV. LCMV infection in the periventricular region of rat forebrain spreads from the ependyma and astrocytes to neurons. (A) On PD8 (4 days postinoculation), infected areas include the choroid plexus (arrowhead), ependymal lining of the ventricle (arrow), and cells of the septal region (double arrowheads) and corpus callosum (*). (D) With the passage of time, infection is cleared from the corpus callosum (*) and deeper portions of the septal region. Infection persists in cells adjacent to the ventricle (arrow). (B) High magnification of boxed area in panel A shows infection of the ependymal lining of the ventricle (double arrowheads) and of cells beneath the ependyma (arrowheads) whose morphology is consistent with astrocytes. (C) On PD18, infection of the ependymal cells (double arrowheads) and astrocytes (arrowheads) is less evident. However, LCMV is now apparent in neuronal cell bodies (arrows). (E) High magnification of the boxed area in panel D shows that the infected cells are no longer astrocytes but are neurons (arrows). The ependymal lining (double arrowheads) no longer shows any evidence of infection. (F) On PD93, viral antigen remains detectable in the cell bodies and processes of many neurons (arrows) near the ependymal wall (double arrowheads). Bars, 1 mm (A and D); 100 μm (B, C, E, and F).

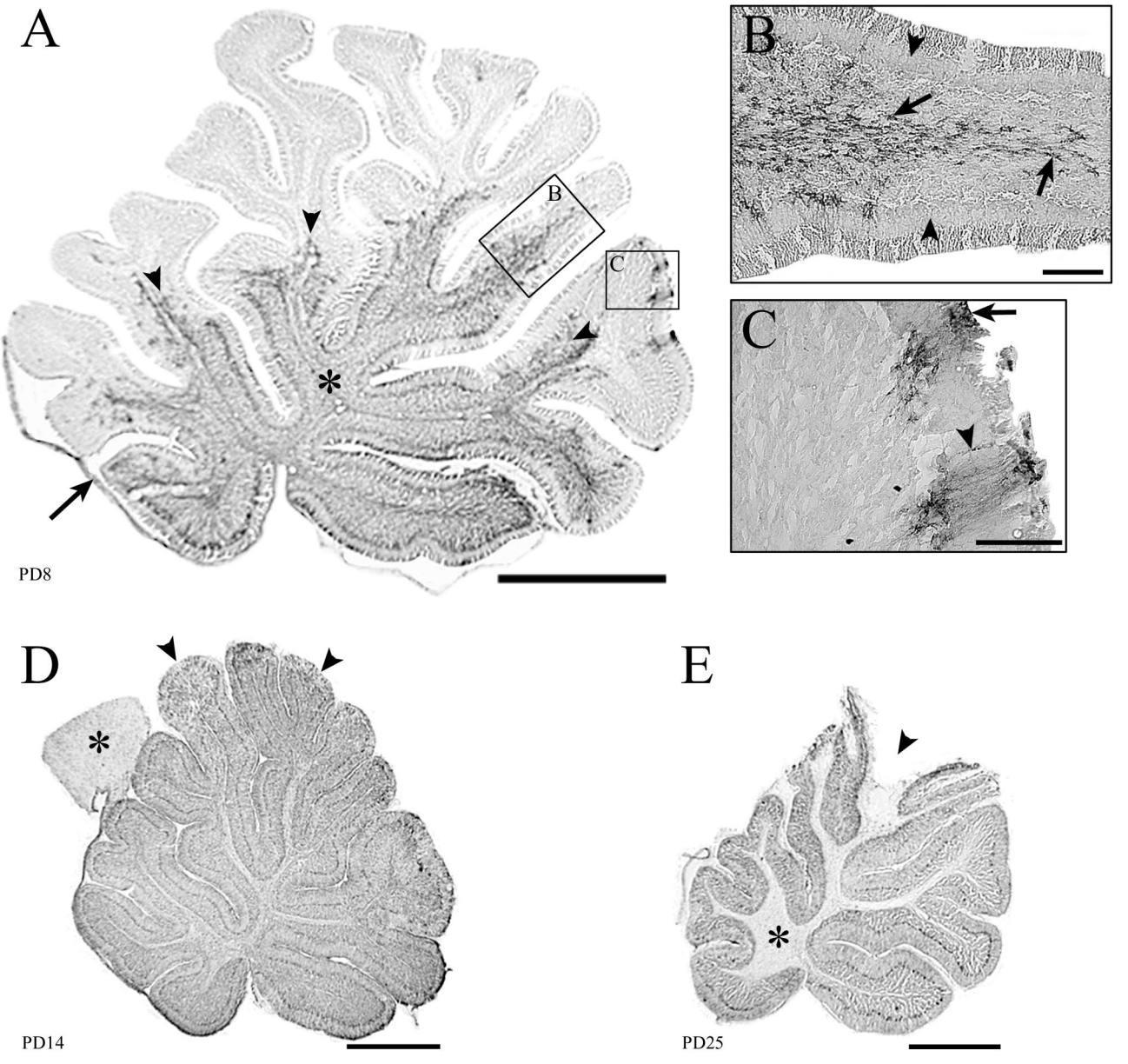

FIG. 3. Fifty-micrometer-thick midsagittal sections through the cerebellum immunohistochemically stained for LCMV. Infection of the cerebellum can spread via astrocytes in the white matter or via the leptomeninges and Bergmann glia. Infection is cleared from glia but persists in cortical neurons. (A) On PD8, the proximal white matter tracts (*) and leptomeninges (arrow) are infected. The arrowheads point to the leading edge of infection, which is spreading from the proximal to the distal portions of the lobules. Boxed areas (B and C) demonstrate the two pathways by which the infection spreads through the cerebellum. (B) Spread of infection via astrocytes within a lobule. Note that the cortex is uninfected (arrowheads), but the white matter astrocytes (arrows) are heavily labeled. (C) Infection spreading into the cerebellum from the leptomeninges (arrow) and Bergmann glia (arrowhead). (D) By PD14, the entire cerebellum is heavily infected, including white and gray matter. In contrast to the cerebellum, the tectal plate (*) of the brain stem has scattered infection of astrocytes only and is thus less intensely labeled. Early pathological changes are visible in the tips of the dorsal lobules (arrowheads), where tissue breakdown is beginning to occur. (E) By PD25, substantial pathology is evident in the dorsal lobules (arrowhead). Infection has been cleared from the white matter (*) but persists in cortical neurons. Bars, 1 mm (A, D, and E); 100 μm (B and C).

regions by PD10 and then became greater in the dorsal cerebellum than in the ventral cerebellum.

Between PD18 and PD25, at a time coincident with clearance of the virus from glial cells, LCMV titer in the cerebellum declined by multiple orders of magnitude. Cerebellar virus titers fell below the limit of detection in some animals by PD38 and in all animals by PD49.

(iii) Pathology in the cerebellum. Approximately 10 days postinoculation (≈PD14), the LCMV infection triggered an acute rapidly progressive destruction of the cerebellum (Fig. 6 and 7). However, despite a nearly homogeneous infection of the cerebellum, not all cerebellar lobules were equally vulnerable to pathological changes. Destruction of the cerebellum always began in the distal tips of the dorsal lobules and pro-

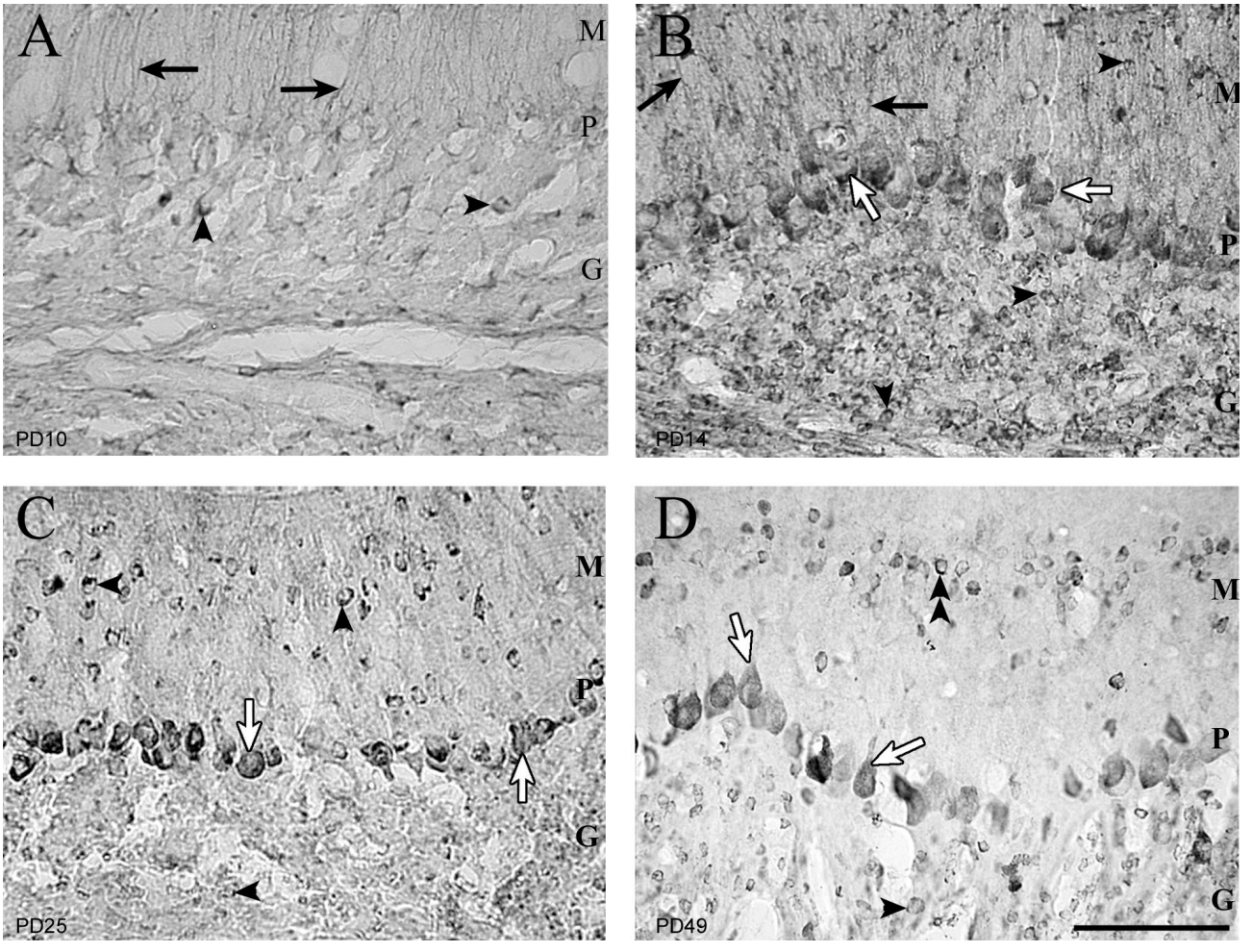

FIG. 4. Fifty-micrometer-thick sections of cerebellar cortex immunohistochemically stained for LCMV. The first cells in the cerebellar cortex infected with LCMV are the Bergmann glia. The virus persists in granule cells and Purkinje cells. (A) On PD10, the only infected cortical cells are the Bergmann glia (arrows) and occasional granule cells (arrowheads). Purkinje cell bodies are not yet infected. (B) Four days later, Purkinje cell bodies (open arrows), granule cells (arrowheads), and Bergmann glia (arrows) are infected. (C) By PD25, the Bergmann glia are no longer infected. Purkinje cell bodies (open arrows) and granule cells (arrowheads) remain infected. (D) On PD49, Purkinje cell bodies and proximal apical dendrites (open arrows) are infected. Granule cells, which have failed to migrate to the granular layer (double arrowheads), remain infected in the molecular layer. Granule cells within the internal granule cell layer (arrowheads) are also persistently infected. M, molecular layer; P, Purkinje cell layer; G, internal granule cell layer. Bar, 100 μm.

gressed over several weeks in a dorsal-to-ventral direction (Fig. 3 and 7). In the course of this acute pathology, in the most severely affected lobules (lobules II to VII), very few Purkinje cells survived, the molecular layer was obliterated, and the cortical architecture was reduced to a disorganized array of cells (Fig. 7). Ultimately, the dorsal lobules of the cerebellum were typically completely destroyed. In contrast, the ventral lobules and the base of the primary fissure were relatively spared (Fig. 7). In these less affected lobules (lobules I, IX, and X and the depth of the primary fissure), a clear trilaminar organization to the cortex remained intact (Fig. 7).

While the ventral lobules consistently displayed less pathological destruction than the dorsal lobules, they were distinctly abnormal nevertheless. As shown in Fig. 4 and 7, not only were the ventral lobules much smaller than their uninfected control counterparts, but they also manifested disrupted neuronal migration. By early adulthood, cerebellar granule cells have normally completed their migration through the molecular layer and into the internal granule cell layer. By this age, no granule cells can normally be identified in the molecular layer. However, in the infected rats, many heterotopic granule cells permanently resided in the molecular layer.

The acute pathology within the cerebellum was self-limited and monophasic. Three to four weeks after the LCMV inoculation, the destructive process within the cerebellum ended. As shown in Fig. 6 and 7, the infected animals were left with only a remnant of cerebellum, but no further ongoing cell loss within the cerebellum was evident.

In order to better characterize the pathological mechanisms underlying the acute cerebellar destruction, sections of cerebellum from LCMV-infected rat pups were stained immunohistochemically for several lymphocytic surface markers. The monoclonal primary antibodies employed recognized either CD4 (mouse anti-rat CD4; Pharmingen) or CD8a (mouse anti-rat

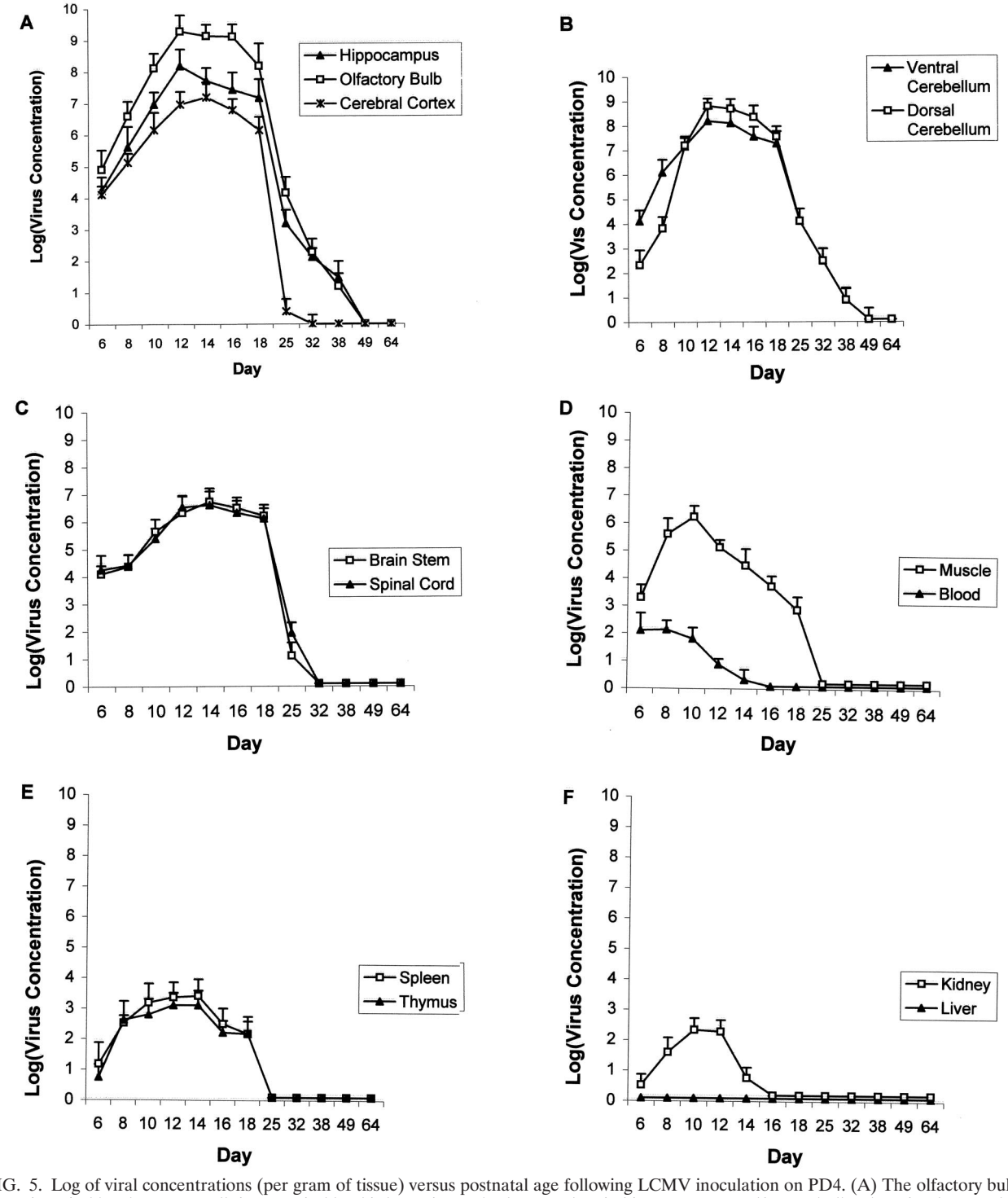

FIG. 5. Log of viral concentrations (per gram of tissue) versus postnatal age following LCMV inoculation on PD4. (A) The olfactory bulb has the heaviest viral burden among all tissues. Viral load is lower in cerebral cortex than in hippocampus or olfactory bulb. There is a large reduction in viral load between PD18 and PD25 in all three brain regions. However, in the cerebral cortex, virus titers fall to near zero on PD25, while virus titers remain substantially greater than zero in the hippocampus and olfactory bulb at this age. Immunohistochemistry demonstrates that reduction in virus titer between PD18 and PD25 reflects clearance of virus from glial cells. The continued presence of infectious virus in the olfactory bulb and hippocampus on PD25 and beyond reflects the persistent infection of neurons. (B) During the initial days following inoculation, virus titers are higher in ventral cerebellum than in dorsal cerebellum. This reflects the ventral-to-dorsal spread of LCMV through the cerebellar lobules. At the peak of infection, the dorsal cerebellum has a higher virus titer than the ventral cerebellum. (C) LCMV infects brain stem and spinal cord but at lower levels than in hippocampus, olfactory bulb, or cerebellum. The nearly total clearance of virus from these tissues by PD25 reflects the fact that only glial cells, not neurons, are infected in these tissues. (D) Following intracerebral inoculation of LCMV, there is a transient low-level viremia. Muscle is more heavily infected than any other extracerebral tissue. (E) Spleen and thymus both contain infectious LCMV particles, though the concentrations do not approach those found in the brain. (F) Low levels of LCMV infection transiently occur in the kidney, but infectious LCMV is never isolated in any quantity from the liver.

CD8a; Pharmingen) antigens. The secondary antibody in each case was horse anti-mouse IgG (Vector Laboratories). Appropriate positive and negative control conditions were included.

Within 8 to 10 days of inoculation with LCMV, infiltration of $CD8^+$ lymphocytes was evident throughout the meninges, ependyma, and choroid plexus. Within several additional days, $CD8^+$ cells were present within the cerebellar parenchyma. However, as shown in Fig. 7, the infiltration of $CD8^+$ cells did not occur simultaneously across the cerebellum. Instead, $CD8^+$ cells were first evident within the tips of the dorsal lobules, which, as noted above, were also the initial site of cerebellar disintegration. Over the course of 2 weeks postinoculation, the density of $CD8^+$ cells increased within the cerebellum. However, the ultimate density of $CD8^+$ cells was not uniform across the cerebellum. While a dense infiltration of $CD8^+$ cells occurred in the dorsal lobules, a far sparser infiltration of these cells occurred ventrally. After PD18, the density of $CD8^+$ cells declined. In contrast to the prominent infiltration of $CD8^+$ cells, no $CD4^+$ cells were observed at any point throughout the time course. Thus, the spatial pattern of cerebellar tissue destruction, in which the dorsal lobules were more severely affected than the ventral lobules, was paralleled by spatial differences in the density of $CD8^+$ but not $CD4^+$ lymphocytes. In addition, as the titer of infectious virus declined, the density of $CD8^+$ cells fell. These results suggest that $CD8^+$ cells but not $CD4^+$ cells play important roles both in the clearance of LCMV and in the acute cerebellar pathology accompanying the infection.

Olfactory bulb. (i) Topography of infection in the olfactory bulb. As was true of the cerebellum, the first cells infected with LCMV within the olfactory bulb were astroglia. The infection then spread from glia to neurons, as it did in the cerebellum and other brain regions (Fig. 8). However, spread of the infection from glial cells to neurons occurred substantially earlier in the olfactory bulb than in any other brain region. As shown in Fig. 8, olfactory mitral cells, which were the first neuronal type of the olfactory bulb to become infected, were labeled by PD8. Infection of olfactory granule cells was evident by PD10. Thus, the infection of olfactory neurons preceded infection of neurons elsewhere, which generally contained viral antigen no earlier than PD12.

By PD18, astroglia, mitral cells, and granule cells of the olfactory bulb were all heavily labeled. These cells of the olfactory bulb were far more susceptible to infection than were the cells of immediately adjacent tissues. As shown in Fig. 8, the olfactory bulb was heavily and homogeneously labeled, while the immediately adjacent olfactory stalk and cerebral cortex were unlabeled.

Following PD18, as occurred elsewhere in the brain, the infection was cleared from glia but persisted in neurons for several months. As was true in the cerebellum, labeling for LCMV dissipated more slowly from the large projection neurons (the mitral cells) than from the small interneurons (the granule cells).

(ii) Viral quantification in the olfactory bulb. As shown in Fig. 5, from the early stages through the height of the infection, the titer of infectious virus was greater in the olfactory bulb than in any other brain region or extracerebral tissue. At the peak of infection, the titer within the olfactory bulb exceeded 10^9 PFU per g of tissue. Only the dorsal cerebellum closely approached this level of infection.

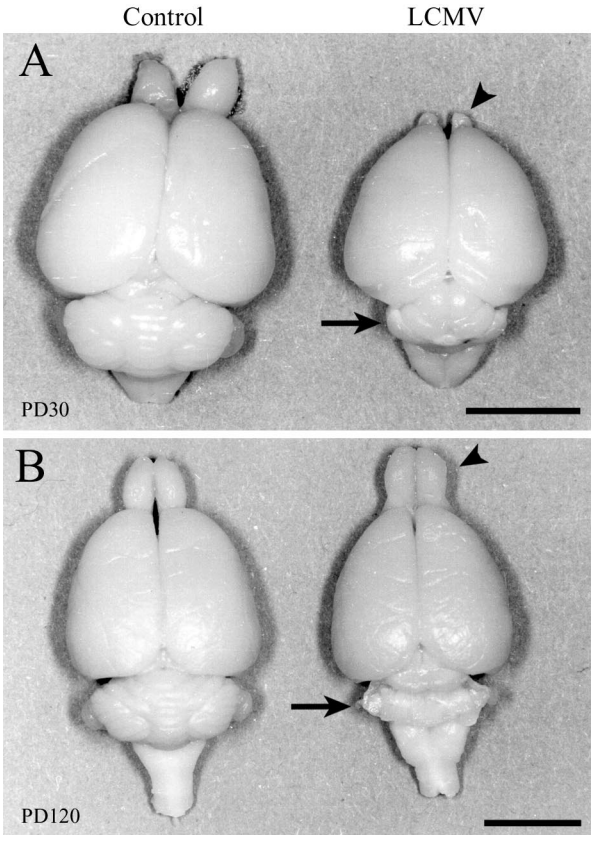

FIG. 6. Dorsal views of control and LCMV-infected rat brains one month (A) and 4 months (B) postinoculation. The effect of LCMV infection on brain growth is region and age dependent. LCMV infection induces a temporary hypoplasia of the olfactory bulbs and a permanent destruction of the cerebellum. (A) On PD30, a substantial microencephaly induced by LCMV infection is evident. While brain growth is globally disrupted, the cerebellum (arrow) and olfactory bulbs (arrowhead) are particularly affected. (B) By PD120, the previously hypoplastic olfactory bulb has rebounded to a normal size (arrowhead), but the cerebellum remains permanently and severely affected (arrow). Bars, 7 mm (A); 7.5 mm (B).

As was true of other brain regions, within the olfactory bulb, a precipitous decline in the quantity of infectious virus occurred between PD18 and PD25 (Fig. 5). This decline in virus titer coincided with the clearance of virus from glial cells. As was true of the cerebellum, olfactory bulb virus titers fell to undetectable levels in some animals by PD38 and in all animals by PD49.

(iii) Pathology in the olfactory bulb. As shown in Fig. 6 and 9, LCMV infection acutely and substantially reduced the size of the olfactory bulbs. However, unlike the cerebellum, where the acute reduction in size was due to a destructive process that obliterated tissue integrity, the reduction in size of the olfactory bulb was due to a hypoplastic process. Figure 9 shows that at 1 month postinoculation, the cross-sectional area of the olfactory bulb was grossly reduced in size relative to uninfected controls. However, as shown in Fig. 9, the cytoarchitecture of the olfactory bulb was preserved, and its cellular constituents

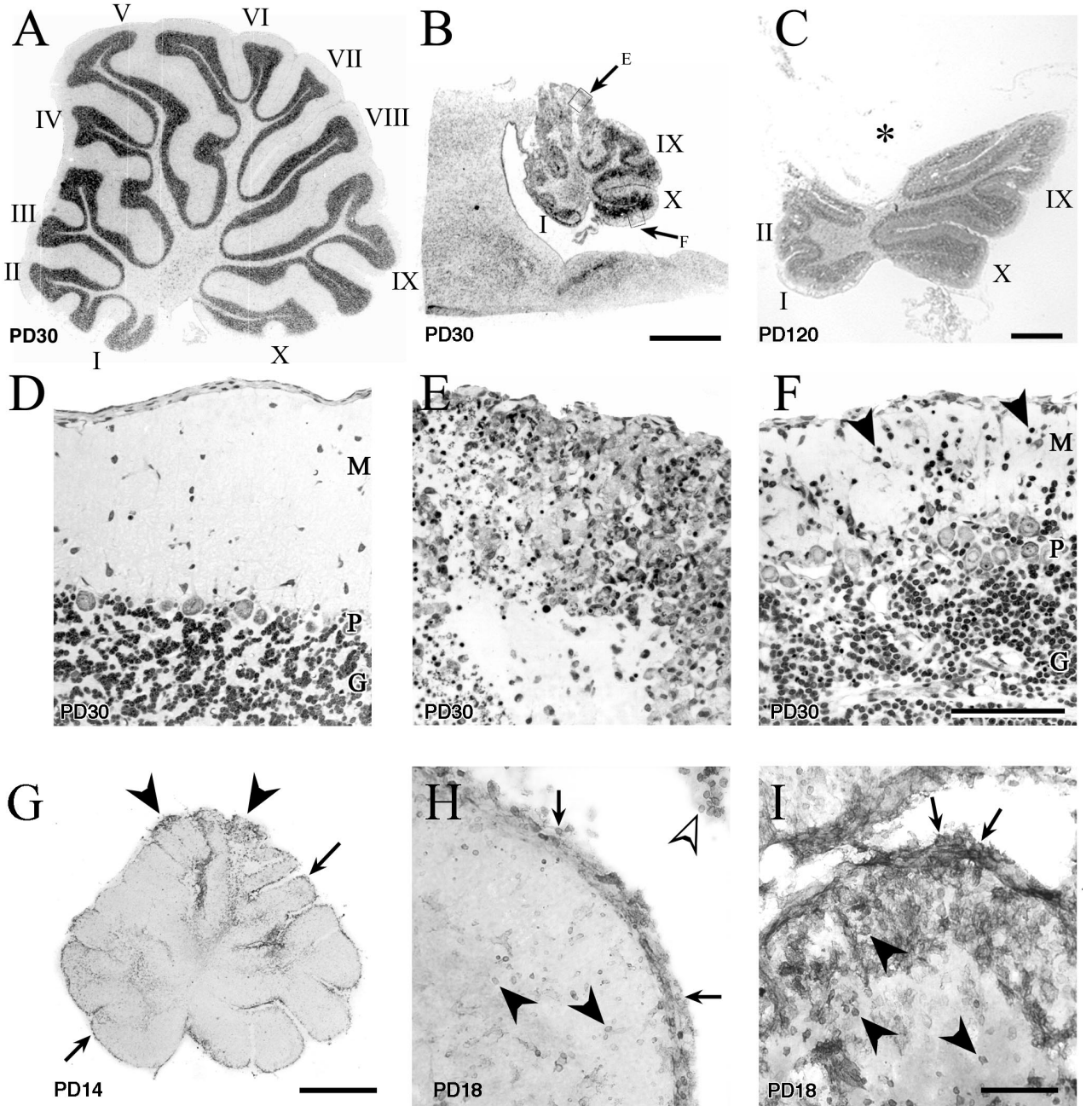

FIG. 7. Midsagittal sections through the cerebellar vermis of control (A and D) and LCMV-infected (B, C, and E to I) littermate rats, demonstrating the acute and long-term pathological changes induced by LCMV infection. The ages of the animals are noted on each panel. Panels A to F are Nissl-stained 2-μm-thick sections, while panels G to I are 50-μm-thick sections stained immunohistochemically for CD8a antigen. Within the cerebellum, LCMV induces a destructive process that is region dependent and permanent and that involves the infiltration of $CD8^+$ lymphocytes. LCMV infection destroys the cytoarchitecture of some lobules and induces a migrational defect in others. (A) The 10 lobules of the control (uninfected) cerebellum are labeled according to the system of Larsell (22). (B) Midsagittal section through the cerebellum of an LCMV-infected rat on PD30, photographed at the same magnification as the control cerebellum in panel A. The severe reduction in the size of the cerebellum induced by LCMV is obvious. Lobules I, IX, and X, which are among the ventral lobules, contain less severe pathological change than do the dorsal lobules. (C) LCMV-infected cerebellum 4 months postinoculation. The dorsal lobules have been obliterated and are now absent. The asterisk (*) denotes the position where the dorsal lobules would normally reside. In contrast, the ventral lobules (I, II, IX, and X) are relatively intact. (D) Control cerebellar cortex demonstrating the normal trilaminar architecture of the cortex. (E) Enlargement of boxed area E from panel B demonstrating the pathological changes within the cerebellar cortex of a dorsal lobule. The cortical architecture has been completely disrupted. No Purkinje cells can be identified, and the molecular layer has been completely destroyed. (F) Enlargement of boxed area F from panel B. In the ventral lobules, all layers of the cortex can be clearly identified and contain many healthy-appearing cells. However, note the abnormal continued presence of granule cells in the molecular layer (arrowheads), indicating a migrational defect. (G) LCMV-infected cerebellum on PD14 immunohistochemically stained for $CD8^+$ cells. Labeling of $CD8^+$ cells is evident along the entire extent of the ependymal and meningeal surfaces of the cerebellum (arrows). In addition, $CD8^+$ cells are prominently present within cerebellar parenchyma at the tips of the dorsal lobules (arrowheads). (H) Lobule I (a ventral lobule) on PD18 has a dense labeling of $CD8^+$ cells over the meningeal surface of the lobule (arrows) and within the choroid plexus (open arrowhead) but relatively few labeled cells within the cerebellar parenchyma (arrowheads). (I) In contrast, a dorsal lobule from the same cerebellum as in panel H has a dense infiltration of $CD8^+$ cells both on the meningeal surface (arrows) and within the parenchyma (arrowheads) of the lobule. M, molecular layer; P, Purkinje cell layer; G, granule cell layer. Bars, 1 mm (A, B, C, and G); 100 μm (D, E, F, H, and I).

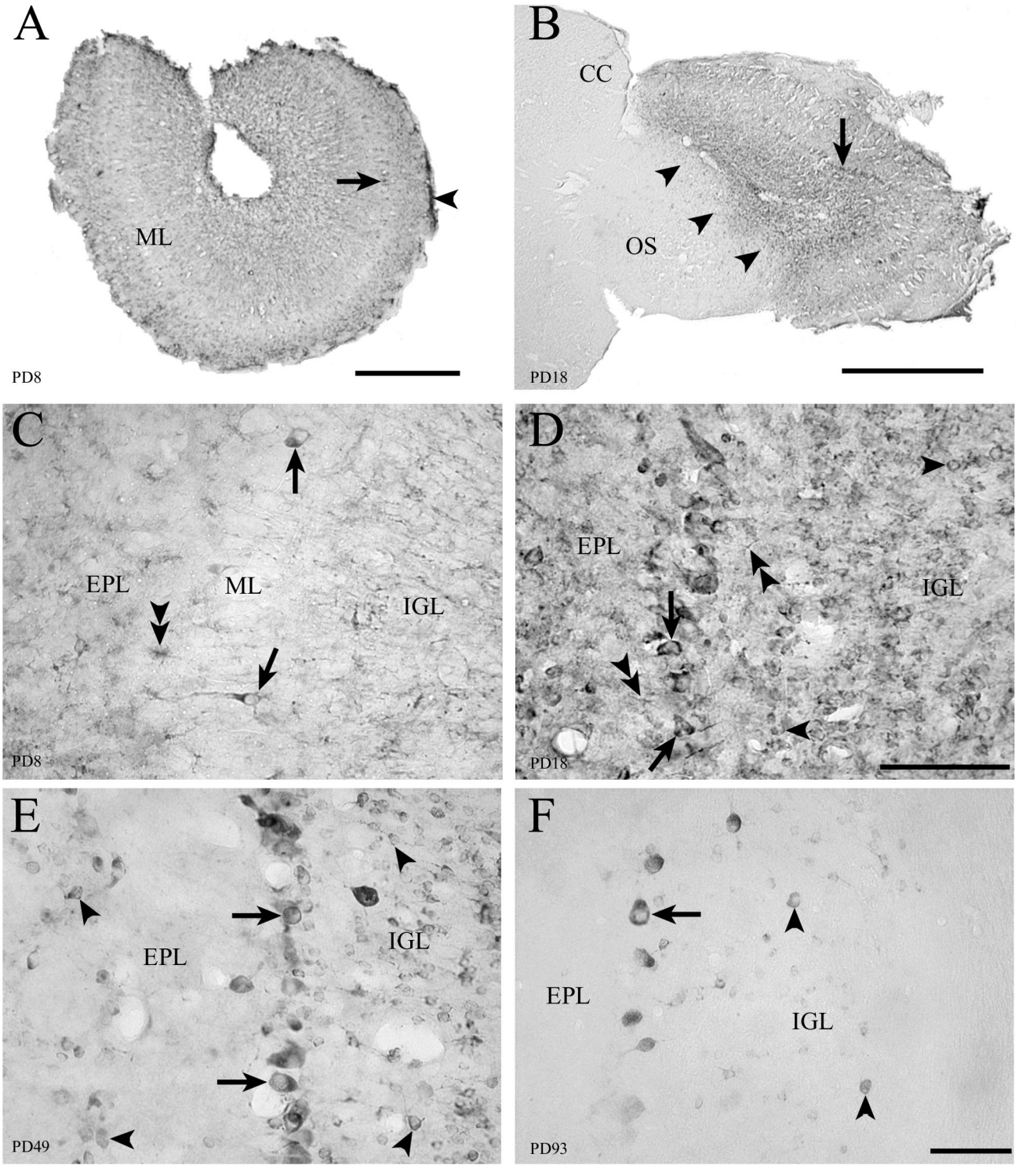

FIG. 8. Fifty-micrometer-thick sections through the olfactory bulb immunohistochemically labeled for LCMV. In the olfactory bulb, infection of LCMV spreads from astrocytes to neurons. Mitral cells are the first neuronal population of the brain to become infected. (A) Low-power image on PD8 shows infection of the leptomeninges (arrowhead) and mitral cell bodies (arrow) as well as parenchyma deep to the mitral cell layer (ML). (B) Arrowheads show a clear demarcation of infection in this parasagittal section of the olfactory bulb on PD18. The olfactory bulb is selectively and heavily infected, while the adjacent olfactory stalk (OS) and cerebral cortex (CC) are spared. Mitral cell bodies are clearly infected (arrow). (C) On PD8, infection principally involves glial cells (double arrowheads). However, a few mitral cells (arrows) are also infected. Mitral cells are the first neuronal population of the brain infected with LCMV. (D) On PD18, glial cells remain infected (double arrowheads). However, the infection has spread beyond glial cells and into large numbers of neurons. Granule cells are now clearly infected (arrowheads), and the proportion of mitral cells (arrows) that are infected has increased. (E) By PD49, the infection has been cleared from glia. However, granule cells (arrowheads) and mitral cells (arrows) remain heavily infected. (F) By adulthood, mitral cells remain heavily infected (arrow) and viral antigen persists in some granule cells (arrowheads). CC, cerebral cortex; EPL, external plexiform layer; IGL, internal granule cell layer; ML, mitral cell layer; OS, olfactory stalk. Bars, 300 μm (A); 1 mm (B); 100 μm (C and D); 80 μm (E and F).

appeared healthy. Furthermore, unlike the cerebellum, in which the acute pathological changes were permanent, the olfactory bulb largely recovered from its initial pathology. As shown in Fig. 6 and 9, by PD120, the cross-sectional area of the previously infected olfactory bulb had regained a nearly normal size. Thus, in contrast to the destructive and permanent pathology of the cerebellum, the hypoplasia of the olfactory bulb is reversible.

The cell count studies demonstrated that the initial hypoplasia of the olfactory bulb was due specifically to a deficit of olfactory granule cells and not mitral cells. As shown in Fig. 10, on PD30, the number of granule cells in the LCMV-infected animals was significantly reduced by 39% relative to controls ($P < 0.0001$). In contrast, the number of mitral cells on PD30 was not significantly affected by the infection. By PD120, the number of granule cells in the infected animals had rebounded and no longer differed significantly from those of controls. Likewise, on PD120, the number of mitral cells in infected and control animals did not differ significantly.

Hippocampus. (i) Topography of infection in the hippocampus. As shown in Fig. 1, infection of the hippocampus began as an infection of astrocytes in patches adjacent to the infected ependymal surface and in the fornix. As was true of all brain regions other than the olfactory bulb, on PD8, only glial cells were infected, and neurons remained unlabeled. The infection then spread from glial cells to neurons. However, not all neuronal populations of the hippocampus were equally susceptible to infection. The only hippocampal neurons ever to be labeled for LCMV were the granule cells of the dentate gyrus and a minority of the adjacent hilar neurons. Hippocampal pyramidal cells were never labeled. The infection was then cleared from glial cells but persisted in the neurons. Labeling of neurons remained strong on PD49 (Fig. 1) and was still evident on PD90, but was absent by PD120.

(ii) Viral quantification in the hippocampus. As was true within the olfactory bulb and ventral cerebellum, LCMV titers rose rapidly and to high levels within the hippocampal formation during the first week postinoculation (Fig. 5). At the peak of the hippocampal infection, which occurred on PD12, the density of infectious virus within the hippocampus exceeded 10^8 PFU per g of tissue. As was true of all brain regions, a sharp decline in virus titer occurred between PD18 and PD25, which, once again, coincided with the clearance of virus from glial cells. The relatively low virus titer on PD25 reflects the continued presence of LCMV within the neurons of the dentate gyrus. As was true within the olfactory bulb and cerebellum, titers of infectious virus within the hippocampus fell to undetectable levels by PD49 in all animals.

(iii) Pathology in the hippocampus. Unlike the acute pathology observed in the cerebellum and olfactory bulb, no acute destructive or hypoplastic process occurred in the hippocampal formation. Instead, a full complement of histologically healthy-appearing neurons was generated. As shown in Fig. 11, at 1 month of age, the size and shape of the hippocampal formation and of its neuronal subpopulations appeared normal. This lack of an acute effect of LCMV on the number of hippocampal cells was confirmed by the cell count studies. Figure 10 shows that, on PD30, the number of CA1 and CA3 pyramidal cells and of dentate granule cells was not affected by the LCMV infection. However, this was followed by a loss of neurons from

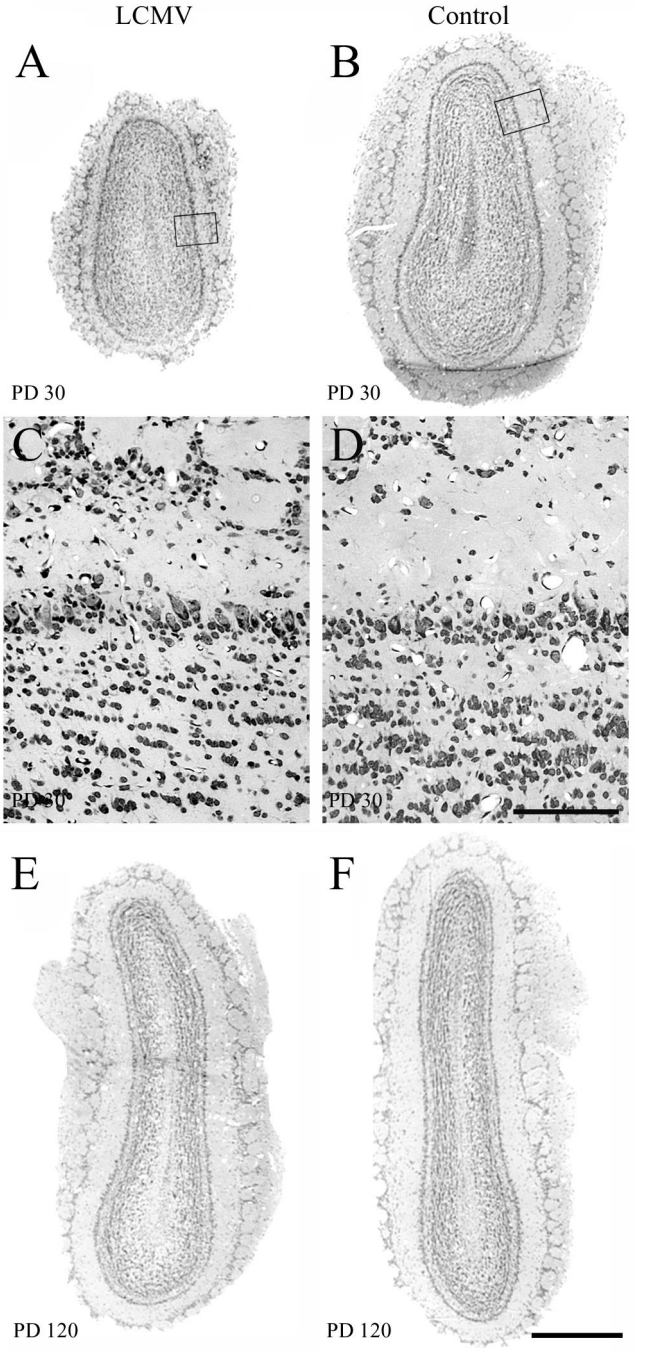

FIG. 9. Two-micrometer-thick Nissl-stained coronal sections through the olfactory bulb of control and LCMV-infected rats at 1 month and 4 months postinoculation. In the olfactory bulb, LCMV infection induces a temporary hypoplasia. At the 1-month time point, the olfactory bulb of the LCMV-infected rat (A) is hypoplastic, relative to that of the control rat (B). C and D are enlargements of the boxed areas from panels A and B, respectively. The cytoarchitecture of the infected olfactory bulb (C) does not differ from that of the uninfected olfactory bulb (D). By 4 months postinoculation, the previously infected olfactory bulb (E) has recovered and does not differ substantially in size from the control olfactory bulb (F). Thus, unlike the cerebellum, the olfactory bulb infected with LCMV does not undergo an acute destructive process. Bars, 500 μm (A, B, E, and F); 100 μm (C and D).

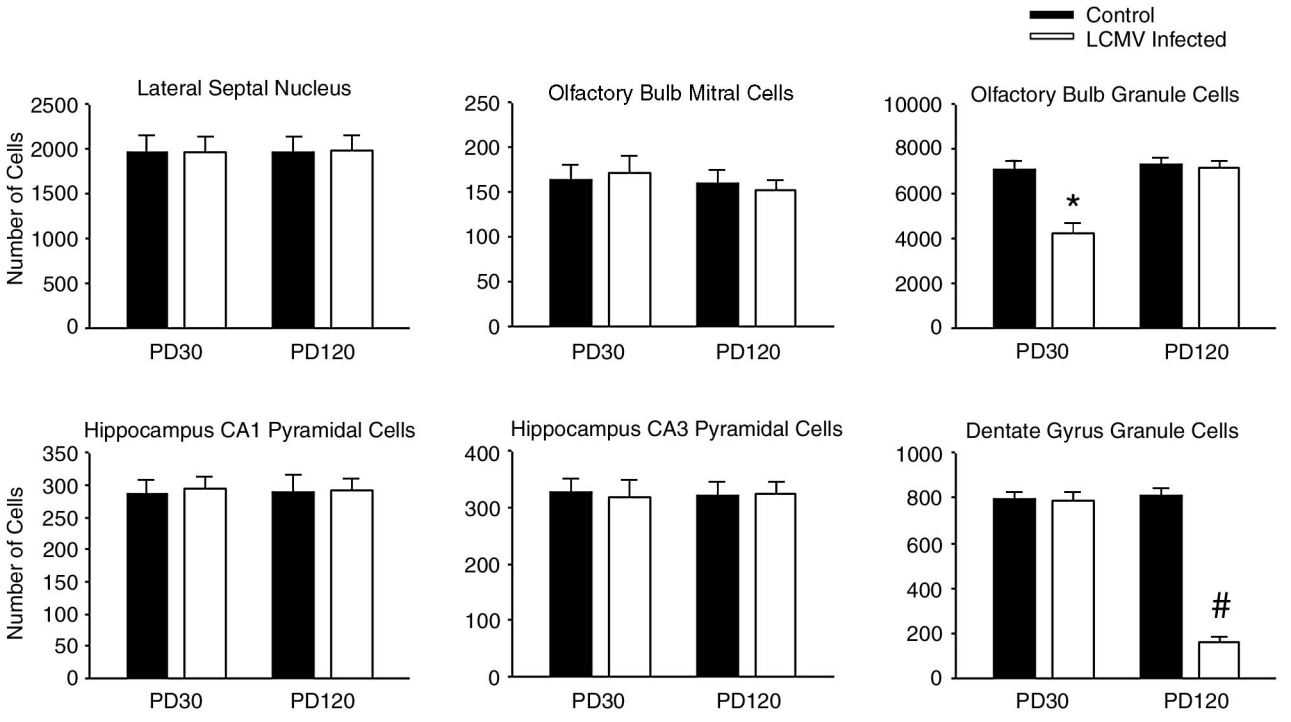

FIG. 10. LCMV infection induces neuronal deficits that are region and age dependent. Cell counts were made from single 2-μm-thick sections through the septum, olfactory bulb, and hippocampal formation. Six neuronal populations within these three regions were quantified in LCMV-infected and control rats on PD30 and on PD120. Within the olfactory bulb, only the granule cells were substantially reduced in number, and the cellular deficits were temporary. By PD120, the number of olfactory granule cells in LCMV-infected animals did not differ from that in controls. In contrast, in the hippocampal formation, the number of dentate granule cells in LCMV-infected animals was normal on PD30 but was significantly reduced by PD120. In further contrast, the number of olfactory mitral cells, hippocampal CA1 and CA3 pyramidal cells, and neurons of the lateral septal nucleus was never significantly affected by LCMV infection. *, significantly different from controls at PD30 and from controls and LCMV-infected animals at PD120 ($P < 0.0001$); #, significantly different from controls and LCMV-infected animals at PD30 and from controls at PD120 ($P < 0.0001$).

the dentate gyrus which progressed over months and eventually resulted in a severe depletion of dentate gyrus granule cells. This substantial drop-out of cells specifically from the dentate gyrus is shown in Fig. 11. By 4 months of age, the granule cell layer, which is normally 10 to 12 cells in thickness, was reduced to only 1 to 3 cells in thickness. The loss of neurons from the dentate gyrus was confirmed by the cell count study. Figure 10 shows that, by PD120, the number of dentate granule cells in the LCMV-infected animals was reduced by 81% relative to uninfected controls ($P < 0.0001$). This delayed drop-out of neurons was limited to the dentate gyrus. The number of hippocampal pyramidal cells was unaffected (Fig. 10).

Periventricular region. (i) Topography of infection in the periventricular region. As shown in Fig. 2, the fourth brain region in which a prominent neuronal infection occurred was the region surrounding the lateral ventricle. This periventricular region included portions of the septum and caudate-putamen (striatum). Infection of this region began with the infection of astrocytes near the infected ventricular surface. As was true of the cerebellum, olfactory bulb, and hippocampus, periventricular neurons initially contained no viral antigen but acquired it by PD12. Following PD18, viral antigen could no longer be detected in glial cells or within the ependyma but persisted in neuronal cell bodies and neurites (Fig. 2). Viral antigen persisted in the periventricular neurons longer than in any other neuronal population and remained detectable as late as PD120, by which time viral antigen was no longer detectable in any other neuronal population.

(ii) Pathology in the periventricular region. Unlike the olfactory bulb and cerebellum, the periventricular region underwent no acute pathological change following LCMV infection. Furthermore, unlike the hippocampus, the periventricular region underwent no evident delayed-onset pathology. The cytoarchitecture of both the septum and the striatum appeared normal at all times. Quantification of neurons within the lateral septal nucleus revealed no acute or long-term deficits in neuron number (Fig. 10). Thus, despite the pattern of glial cell and subsequent neuronal infection, a pattern which induced some form of pathology in each of the other three infected brain regions, no appreciable pathological changes occurred in the periventricular region.

Regional differences in viral load and in neuronal loss. A principal goal of this study was to determine whether individual regions of the CNS are differentially vulnerable to LCMV infection and whether the severity of pathology among infected regions is dependent on regional viral load. As shown in Fig. 5, strong regional differences existed across the CNS, not only in the magnitude of the peak viral burdens, but also in the rapidity with which regions became infected and in the timing of viral clearance. Because there were no significant differences in virus titer between the right and left sides of the cerebral

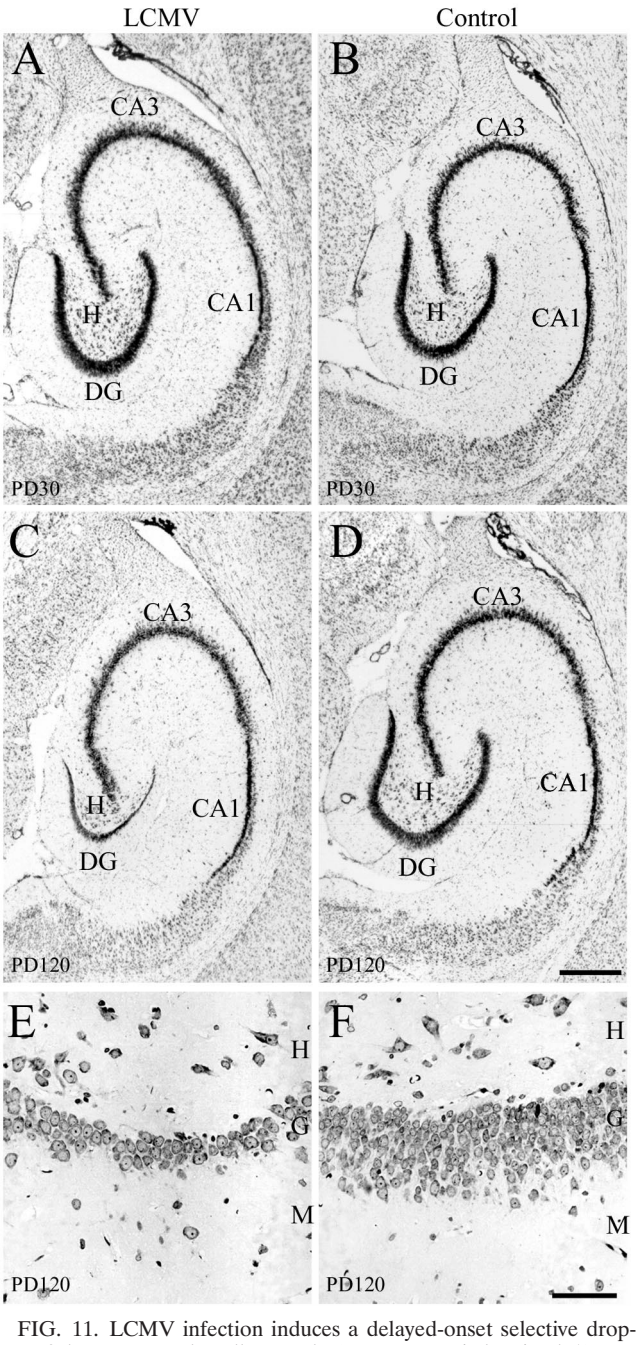

FIG. 11. LCMV infection induces a delayed-onset selective drop-out of dentate granule cells. Panels A to D are Nissl-stained 50-μm-thick sections cut in the horizontal plane through the hippocampal formation at the midtemporal level of control and LCMV-infected rats 1 month and 4 months postinoculation. At the 1-month time point, the hippocampal formation of infected rats (A) does not appear histologically different from that of controls (B). A full complement of pyramidal and granule cells is present despite a selective and heavy infection of the granule cells. However, at 4 months postinoculation (C), the granule cell layer of the dentate gyrus is markedly reduced in width relative to the 4-month-old control (D). The LCMV-induced cell loss is selective to the dentate gyrus, as the CA1 and CA3 pyramidal cell populations are unaffected. Panels E and F are 2-μm-thick cresyl violet-stained horizontal sections through the dentate gyrus from LCMV-infected (E) and control (F) rats 4 months postinoculation. In the LCMV-infected rats, the substantially reduced width of the granule cell layer is due to a massive loss of granule cells. Whereas the granule cell layer of the dentate gyrus is normally 10 to 12 cells thick (F), in the LCMV-infected animal, the dentate gyrus has been reduced to 1 to 3 cells in thickness (E). M, molecular layer; G, granule cell layer; H, hilus; CA1, CA1 pyramidal cells; CA3, CA3 pyramidal cells; DG, dentate gyrus granule cells. Bars, 500 μm (A to D); 50 μm (E and F).

cortex, hippocampus, or olfactory bulb at any age, values for the two sides were averaged together for the statistical analyses and for the plots shown in Fig. 5.

Early in the course of infection (on PD8 and on PD10), virus titer was significantly greater in the olfactory bulb than in any other region ($P < 0.01$). Likewise, during the early stages of infection, the hippocampus and the ventral cerebellum contained titers of LCMV that significantly exceeded virus titers in most other CNS regions. In contrast to the ventral cerebellum, the dorsal cerebellum initially contained titers of LCMV that were significantly lower than those of all other brain regions ($P < 0.01$). This difference in virus titer between the dorsal and ventral lobules in the early stages of infection reflected the ventral-to-dorsal spread of the virus evident in Fig. 3.

Within all CNS regions, virus titers reached maximum values on either PD12 or PD14. At the peak of infection, virus titers within the olfactory bulb were significantly greater than in all other CNS regions ($P < 0.001$) except for the dorsal cerebellum. During this period of peak infection, virus titers within the brain regions in which both neurons and glial cells became infected (olfactory bulb, hippocampus, and cerebellum) were significantly greater than were the virus titers in the brain regions within which the infection was limited to glial cells (cerebral cortex and brainstem) ($P < 0.0001$).

Between PD18 and PD25, virus titers fell by multiple orders of magnitude in all CNS regions. As demonstrated immunohistochemically, this decline in virus titer corresponded with the clearance of the virus from glial cells. In the brain regions in which neurons were not infected (brain stem and cerebral cortex), the virus titers fell below detection after PD18. In the brain regions in which neurons were infected (cerebellum, olfactory bulb, and hippocampus), the virus titers fell multiple orders of magnitude after PD18 to low but detectable values. The relatively low titers in the hippocampus, cerebellum, and olfactory bulb on PD25 and beyond reflected the persistent infection of neurons. By PD25, virus titers in brain regions containing persistently infected neurons were significantly higher than virus titers in brain regions in which neurons were not infected ($P < 0.005$). These results support two conclusions. First, glial cells are the principal site of viral propagation. Second, strong regional differences exist among brain regions in the peak viral burden achieved and in the rate of viral clearance.

Substantial regional differences existed, not only in viral content, but also in the timing and severity of neuron loss (Fig. 10). As described earlier, the infection induced an early deficit in olfactory bulb granule cells, from which the infected animals recovered, and a delayed-onset loss of granule cells from the dentate gyrus. In contrast, hippocampal pyramidal cells, olfactory mitral cells, and neurons of the lateral septal nucleus were never reduced in number by the infection. These findings confirm not only that neuron loss occurs in this infection and that the severity of the cell loss varies by region and by neuronal

subpopulation but also that the pattern of cell loss is a function of age.

As shown in Fig. 5, LCMV infectivity varied substantially, not only among CNS regions but also among regions outside the nervous system. Intracranial injection of LCMV induced a transient low-level viremia, which peaked at or prior to PD6 and was cleared by PD16. The viremia was accompanied by infection of most but not all other systemic tissues. As was true of all CNS tissues, virus titers fell precipitously in muscle, spleen, and thymus between PD18 and PD25. In kidney, virus was cleared earlier. The ANOVA of peak viral concentrations verified that LCMV infectivity varied significantly among the extra-CNS tissues ($P < 0.001$). Peak viral concentration in muscle exceeded that of any other non-CNS tissue ($P < 0.001$) and closely approached the concentrations achieved in some CNS regions. In contrast, infection of the liver was not observed. Within the liver, concentrations of LCMV remained undetectable throughout the time course.

The consistent finding of undetectable LCMV titers within the liver raised the possibility that the absence of plaques in the assay was not due to the absence of virus, but that homogenization of liver cells may kill the virus that is present. To test this hypothesis, 10^5 PFU of stock LCMV was added to 0.5 g of liver obtained from an uninfected PD10 rat pup. Plaque assays were performed on this mixture. The results yielded a "titer" of nearly 2×10^5 PFU per g of liver. This result demonstrates that exposure of LCMV to homogenized liver does not kill the virus and suggests that the undetectable LCMV titer within the livers of infected rat pups was due to absence of liver infection.

DISCUSSION

This study yielded three important new findings. First, glial cells play a major role in the propagation and spread of LCMV infection throughout the developing rat brain. Second, LCMV infects neurons in four discrete regions of the developing brain and induces unique pathological changes in each of those regions. Third, the olfactory bulb recovers fully from the neuronal deficits induced by LCMV infection, while other infected brain regions do not.

(i) Glial cells play a major role in the pathogenesis of LCMV in the developing rat brain. Glial cells are the first cells of the brain parenchyma infected with LCMV. While the morphology, location, and GFAP staining characteristics identify the infected glial cells as predominantly astrocytes and Bergmann glia, a proportion of the cells may be microglia.

The initially infected glial cells occupy regions near the ependymal and meningeal surfaces. Astrocytes and Bergmann glia in these locations extend processes to the brain surfaces (3, 25). These earliest-infected glial cells probably derive their vulnerability from the proximity of their processes to the heavily infected ependyma and leptomeninges.

Glial cells then provide the network along which LCMV spreads throughout the brain to reach the multiple anatomically isolated regions of neuronal vulnerability. The finding that glial cells are heavily infected prior to neuronal infection strongly suggests that the virus reaches susceptible neurons via glial-neuronal interactions. For example, in the cerebellum, Bergmann glia contain large quantities of viral antigen before Purkinje cells or granule cells contain any. Bergmann glia are intimately associated with Purkinje cells and form the scaffolding along which granule cells migrate (3, 40). Thus, the physical proximity of Bergmann glia to Purkinje cells and granule cells provides the opportunity for spread of infection from glia to neurons.

Glial cells not only are the portal of entry of LCMV into the brain parenchyma and the conduit through which the virus reaches neurons but also are the principal site of viral propagation. However, despite the robust infection of glial cells, it is in the brain regions in which neurons are infected that pathological changes occur.

This is the first study to demonstrate the central role of glial cells in LCMV infection of the developing brain. Pearce and coauthors (37) found that rats infected with LCMV on PD4 and immunosuppressed with antilymphocyte serum throughout life had evidence of infected astrocytes on PD90. In contrast, infected rats that were not immunosuppressed did not have infected astrocytes on PD90. The authors concluded that the immunosuppression allowed spread of infection beyond neurons and into glia. However, earlier time points were not examined. Our results show that glial cells are normally infected early in the course of infection and subsequently clear the infection, while the virus persists in neurons. These results suggest a different interpretation of Pearce's findings: the LCMV-infected glial cells observed in immunocompromised adult rats contained viral antigen not because immunosuppression allowed spread of infection to glia but because immunosuppression allowed persistence of virus in glial cells that would normally have been cleared of the infection. Thus, the conjunction of this and Pearce's study allows the further conclusion that lymphocytes are required to clear LCMV from glial cells. This conclusion is further strengthened by our finding that the infiltration of $CD8^+$ lymphocytes within brain parenchyma parallels viral clearance from glia.

(ii) LCMV infects neurons in four specific brain regions and induces unique pathological changes in each region. Several decades ago, Monjan and coworkers recognized that LCMV specifically infects neurons of the cerebellum, olfactory bulb, and dentate gyrus (30, 32, 34). Neuronal infection outside of these three brain regions was noted to be rare. The unique feature shared by these three brain regions in the neonatal rat is the presence of a mitotically active granule cell population.

The present study confirmed the marked vulnerability of the cerebellum, olfactory bulb, and dentate gyrus to neuronal infection by LCMV. In addition, we have demonstrated that the neurons of the periventricular region are also susceptible to LCMV infection. Interestingly, the periventricular region of the postnatal rat also retains a population of mitotically active cells (26, 35). This area of active mitosis, which gives rise to both neurons and glia (24, 27), lies adjacent to the walls of the lateral ventricles, which is precisely the location of neurons vulnerable to LCMV. Thus, LCMV infects neurons in four specific brain regions of the neonatal rat, and the unique feature shared among all four regions is the presence of mitotically active neuronal stem cells.

LCMV infects only brain regions that contain a population of mitotically active neuronal precursors, and, conversely, all brain regions containing mitotically active neuronal precursors are infected. However, within infected regions, not all infected neurons are mitotically active. Purkinje cells and olfactory mi-

tral cells are postmitotic in the neonatal rat but are susceptible to infection. It is likely that the metabolic machinery accompanying cellular mitosis facilitates propagation of LCMV and that LCMV spreads from mitotically active cells containing this machinery to postmitotic cells adjacent to them.

The acute destruction of the cerebellum in LCMV-infected neonatal rats has been documented previously (4, 30, 33). This study extended that finding by demonstrating lobular differences across the cerebellar vermis in the vulnerability to and time course of tissue destruction and by showing that the acute pathology in the cerebellum is likely mediated by $CD8^+$ lymphocytes.

Pathological disintegration of the cerebellar vermis begins at the tips of the dorsal lobules and progresses ventrally. Ultimately, the dorsal lobules are completely destroyed, while the ventral lobules are relatively spared. This pattern of differential pathological severity across the cerebellar vermis matches the spatial ontogeny of histologic maturation. Throughout the early postnatal period, the cerebellar cortex undergoes substantial developmental changes, including the generation and migration of granule cells. However, marked regional differences exist across the cerebellar vermis such that cortical histogenesis is more advanced in some regions than in others (1, 2, 8). The ventral lobules are consistently advanced in their maturational state, while the tips of the dorsal lobules are histologically the least mature region of the developing cerebellum. Thus, the least mature region of the cerebellum is most vulnerable to LCMV-induced pathology, while the most mature region is relatively spared.

These regional differences in vulnerability may be a function of mitotic activity. Since the dorsal lobules are histologically the least mature in the neonatal rat, they are the most mitotically active (1). Since LCMV preferentially infects dividing neurons, the dorsal lobules may be more vulnerable to infection. This was confirmed in the virus titer analysis, where, at the peak of infection, the dorsal cerebellum had a higher viral load than did the ventral cerebellum.

Within the lobules that are not acutely destroyed, there is a second form of pathology, which is disruption of granule cell migration. Under normal conditions, newly generated granule cells utilize the radially oriented fibers of the Bergmann glia to navigate into the internal granule cell layer (40). In LCMV-infected rats, the migration of granule cells is disrupted, and granule cells are ectopically located within the molecular layer. This disrupted migration may be due to the corruption of Bergmann glia, which are early targets of LCMV infection.

The marked differences across the cerebellum in severity of LCMV-induced pathology suggest that the pathological mechanisms in the dorsal and ventral lobules may differ from each other. The obliteration of the dorsal lobules and death of all its resident neurons clearly demonstrate that the pathological process there is one of destruction. In contrast, the neuronal migrational disturbance and reduced size of the ventral lobules suggest a pathological process of developmental arrest. The pathological processes in the dorsal and ventral cerebellar lobules are probably both immune mediated (33). However, the cellular and molecular mechanisms underlying the pathological changes in the two regions may differ considerably.

Like the cerebellum, the infected olfactory bulb also undergoes acute pathological changes. However, the nature and outcome of the pathology in the olfactory bulb are very different from those of the cerebellum. LCMV infection induces an acute hypoplasia of the olfactory bulb. Unlike the cerebellum, the olfactory bulb does not undergo a destructive process. The cytoarchitecture of the olfactory bulb is preserved and its cellular constituents remain histologically healthy. Furthermore, unlike the cerebellum, the olfactory bulb regains a normal size and shape by adulthood.

In contrast to the cerebellum and olfactory bulb, the hippocampus does not undergo any acute pathological change despite a heavy infection of dentate granule cells. Instead, a full complement of granule cells are generated. However, this is followed by a delayed-onset loss of granule cells, which progresses over months and eventually results in a severe and specific depletion of dentate granule cells. This delayed cellular mortality is not immune mediated and may involve excitotoxicity (37, 38, 39).

The fourth brain region in which neurons become infected, the periventricular region, undergoes neither acute nor delayed-onset pathology. No neuronal loss or migrational disturbance is evident at any time in the periventricular region.

Why four brain regions infected simultaneously with a single viral species would differ so markedly from each other in pathological consequence is unknown. The explanation is not likely related to differences in viral load, as each of the regions was heavily infected. At the peak of infection, the olfactory bulb carried a higher viral load than the cerebellum but was less severely affected pathologically.

(iii) Unlike the cerebellum, the olfactory bulb fully recovers from the acute pathological changes induced by LCMV. It is unlikely that the olfactory bulb's reduction in size during LCMV infection is due to neuronal death because, unlike the cerebellum, cell death in the olfactory bulb was never observed. Rather, the reduction in size is probably due to a virus-induced arrest of granule cell generation, from which the animal recovers as the virus is cleared. Granule cell production normally continues throughout postnatal life, providing the opportunity for the olfactory bulb to acquire a normal complement of granule cells despite an early deficit (20).

It is notable that the dentate gyrus also normally continues to generate new neurons throughout postnatal life (41) but suffers a long-term loss of neurons following LCMV infection, rather than a recovery. This finding suggests that neuronal precursors are killed by LCMV in the dentate gyrus while they are spared in the olfactory bulb and further underscores the dramatic regional differences in LCMV-induced pathology and outcome.

The results of the present study also shed light on several aspects of human congenital LCMV infection. First, cortical dysplasia consistent with abnormal neuronal migration may occur in children with congenital LCMV infection (28, 46). This study demonstrated that neuronal migration can be disrupted by LCMV infection and suggested that the mechanism involves infection of radial glia. Second, unlike most other congenital infections, LCMV infection is not associated with hepatomegaly or abnormal elevations in liver enzyme levels in serum (6). This study provides a biological explanation for this clinical observation by demonstrating that the developing liver is not susceptible to LCMV infection. Third, periventricular calcifications are often observed in human congenital LCMV

infection (5, 46). This study explains the location of these calcifications by demonstrating that periventricular neurons are particularly susceptible to LCMV infection. Fourth, some infants congenitally infected with LCMV are highly symptomatic neurologically during the neonatal period but recover with time and are left with only moderate neurologic impairment (D. J. Bonthius, unpublished observation). The neuropathology in these infants may reflect the events in the rat olfactory bulb, where LCMV induces substantial acute pathology from which the animal recovers. Finally, a pregnant woman infected with LCMV usually develops only aseptic meningitis, and not encephalitis, while the fetal brain undergoes widespread infection (21, 46). Multiple studies have demonstrated that adult rodents infected with LCMV develop meningitis but that the brain parenchyma is spared infection (11). In contrast, this study demonstrated that the developing brain parenchyma is infected with LCMV and that viral propagation and spread occur principally in astrocytes. Taken together, the results suggest that the differential effects of LCMV infection on the human mother and fetus are due to age-dependent differences in virus-astroglia interactions.

ACKNOWLEDGMENTS

This research was supported by Public Health Service grants P30-HD27748 from the National Institute of Child Health and Human Development and K08 NS02007-01A2 from the National Institute of Neurologic Disorders and Stroke, by research grant 1-01-217 from the March of Dimes Birth Defects Foundation, by the John Martin Fund for Neuroanatomic Research, by a Carver Medical Research Initiative Grant, by research grants from the Children's Miracle Network, and by a Young Investigator Award from the Child Neurology Society to D.J.B. M.J.B. was supported by NIH grants AI39808 and MH61224.

We thank Stanley Perlman for advice and encouragement. We are grateful to Gary Van Hoesen for the use of microscopy equipment. We thank Charles Grose and Jose Assouline for critical reviews of the manuscript.

REFERENCES

1. **Altman, J.** 1969. Autoradiographic and histological studies of postnatal neurogenesis. III. Dating the time of production and onset of differentiation of cerebellar microneurons in rats. J. Comp. Neurol. **136:**269–294.
2. **Altman, J.** 1972. Postnatal development of the cerebellar cortex in the rat. II. Phases in the maturation of Purkinje cells and of the molecular layer. J. Comp. Neurol. **145:**399–464.
3. **Altman, J., and S. A. Bayer.** 1997. Development of the cerebellar system, p. 498–523. CRC Press, New York, N.Y.
4. **Baldridge, J. R., B. D. Pearce, B. S. Parekh, and M. J. Buchmeier.** 1993. Teratogenic effects of neonatal arenavirus infection on the developing rat cerebellum are abrogated by passive immunotherapy. J. Virol. **197:**669–677.
5. **Barton, L. L., S. C. Budd, W. S. Morfitt, C. J. Peters, T. G. Ksiazek, R. F. Schindler, and M. T. Yoshino.** 1993. Congenital lymphocytic choriomeningitis virus infection in twins. Pediatr. Infect. Dis. J. **12:**942–946.
6. **Barton, L. L., and M. B. Mets.** 2001. Congenital lymphocytic choriomeningitis virus infection: decade of rediscovery. Clin. Infect. Dis. **33:**370–374.
7. **Barton, L. L., C. J. Peters, and T. G. Ksiazek.** 1995. Lymphocytic choriomeningitis virus: an unrecognized teratogenic pathogen. Emerg. Infect. Dis. **1:**152–153.
8. **Bonthius, D. J., and J. R. West.** 1990. Alcohol-induced neuronal loss in developing rats: increased brain damage with binge exposure. Alcohol Clin. Exp. Res. **14:**107–118.
9. **Bonthius, D. J., and J. R. West.** 1991. Permanent neuronal deficits in rats exposed to alcohol during the brain growth spurt. Teratology **44:**147–163.
10. **Bonthius, D. J., and J. R. West.** 1991. Acute and long-term neuronal deficits in the rat olfactory bulb following alcohol exposure during the brain growth spurt. Neurotoxicol. Teratol. **13:**611–619.
11. **Buchmeier, M. J., and A. J. Zajac.** 1999. Lymphocytic choriomeningitis virus, p. 575–606. *In* R. Ahmed and I. Chen (ed.), Persistent viral infections. Wiley, New York, N.Y.
12. **Childs, J. E., G. E. Glass, T. G. Ksiazek, C. A. Rossi, J. G. Barrera Oro, and J. W. Leduc.** 1991. Human-rodent contact and infection with lymphocytic choriomeningitis and Seoul viruses in an intercity population. Am. J. Trop. Med. Hyg. **44:**117–121.
13. **Cole, G. A., D. H. Gilden, A. A. Monjan, and N. Nathanson.** 1971. Lymphocytic choriomeningitis virus: pathogenesis of acute central nervous system disease. Fed. Proc. **30:**1831–1841.
14. **del Cerro, M., D. A. Grover, A. A. Monjan, C. J. Pfau, and J. E. DeMatte.** 1982. Chronic retinitis in rats infected as neonates with lymphocytic choriomeningitis virus: a clinical, histopathologic, and electroretinographic study. Investig. Ophthalmol. Vis. Sci. **23:**697–714.
15. **Dobbing, J.** 1981. The later development of the brain and its vulnerability, p. 331–336. *In* J. A. Davis and J. Dobbing (ed.), Scientific foundations of paediatrics. Heinemann, London, England.
16. **Dobbing, J., and J. Sands.** 1973. Quantitative growth and development of the human brain. Arch. Dis. Child. **48:**757–767.
17. **Dobbing, J., and J. Sands.** 1979. Comparative aspects of the brain growth spurt. Early Hum. Dev. **3:**89–93.
18. **Enders, G., M. Varho-Gobel, J. Lohler, E. Terletskaia-Ladwig, and M. Eggers.** 1999. Congenital lymphocytic choriomeningitis virus infection: an underdiagnosed disease. Pediatr. Infect. Dis. J. **18:**652–655.
19. **Hinds, J. W., and N. A. McNelly.** 1977. Aging of the rat olfactory bulb: growth and atrophy of constituent layers and changes in size and number of mitral cells. J. Comp. Neurol. **171:**345–368.
20. **Kaplan, M. S., N. A. McNelly, and J. W. Hinds.** 1985. Population dynamics of adult-formed granule neurons of the rat olfactory bulb. J. Comp. Neurol. **239:**117–125.
21. **Komrower, G. M., B. L. Williams, and P. B. Stones.** 1955. Lymphocytic choriomeningitis in the newborn. Probable transplacental infection. Lancet **i:**697–698.
22. **Larsell, O.** 1952. The morphogenesis and adult pattern of the lobules and fissures of the cerebellum of the white rat. J. Comp. Neurol. **97:**281–356.
23. **Larson, P. D., S. A. Chartrand, K. M. Tomashek, L. G. Hauser, and T. G. Ksiazek.** 1993. Hydrocephalus complicating lymphocytic choriomeningitis virus infection. Pediatr. Infect. Dis. J. **12:**528–531.
24. **Levison, S. W., and J. E. Goldman.** 1993. Both oligodendrocytes and astrocytes develop from progenitors in the subventricular zone of postnatal rat forebrain. Neuron **10:**201–212.
25. **Levitt, P., and P. Rakic.** 1980. Immunoperoxidase localization of GFAP in radial glial cells and astrocytes of the developing rhesus monkey brain. J. Comp. Neurol. **193:**815–840.
26. **Lois, C., and A. Alvarez-Buylla.** 1993. Proliferating subventricular zone cells in the adult mammalian forebrain can differentiate into neurons and glia. Proc. Natl. Acad. Sci. USA **90:**2074–2077.
27. **Luskin, M. B.** 1993. Restricted proliferation and migration of postnatally generated neurons derived from the forebrain subventricular zone. Neuron **11:**173–189.
28. **Mets, M. B., L. L. Barton, A. S. Khan, and T. G. Ksiazek.** 2000. Lymphocytic choriomeningitis virus: an underdiagnosed cause of congenital chorioretinitis. Am. J. Ophthalmol. **130:**209–215.
29. **Meyer, H. M., R. T. Johnson, I. P. Crawford, H. E. Dascomb, and N. G. Rogers.** 1960. Central nervous system syndromes of "viral" etiology: a study of 713 cases. Am. J. Med. **29:**334–347.
30. **Monjan, A. A., D. H. Gilden, G. A. Cole, and N. Nathanson.** 1971. Cerebellar hypoplasia in neonatal rats caused by lymphocytic choriomeningitis virus. Science **171:**194–196.
31. **Monjan, A. A., L. S. Bohl, and G. A. Hudgens.** 1975. Neurobiology of LCM virus infection in rodents. Bull. W. H. O. **52:**487–492.
32. **Monjan, A. A., G. A. Cole, D. H. Gilden, and N. Nathanson.** 1973. Pathogenesis of cerebellar hypoplasia produced by lymphocytic choriomeningitis virus infection of neonatal rats. J. Neuropathol. Exp. Neurol. **32:**110–124.
33. **Monjan, A. A., G. A. Cole, and N. Nathanson.** 1974. Pathogenesis of cerebellar hypoplasia produced by lymphocytic choriomeningitis virus infection of neonatal rats: protective effect of immunosuppression with anti-lymphoid serum. Infect. Immun. **10:**499–502.
34. **Monjan, A. A., G. A. Cole, and N. Nathanson.** 1973. Pathogenesis of LCM disease in the rat, p. 195–206. *In* F. Lehmann-Grube (ed.), Lymphocytic choriomeningitis virus and other arena viruses. Springer-Verlag, New York, N.Y.
35. **Morshead, C. I., and D. Van der Kooy.** 1992. Postmitotic death is the fate of constitutively proliferating cells in the subependymal layer of the adult mouse brain. J. Neurosci. **12:**249–256.
36. **Paxinos, G., and C. Watson.** 1998. The rat brain in stereotaxic coordinates. Academic Press, San Diego, Calif..
37. **Pearce, B. D., C. L. Po, T. L. Pisell, and A. H. Miller.** 1999. Lymphocytic responses and the gradual hippocampal neuron loss following infection with lymphocytic choriomeningitis virus (LCMV). J. Neuroimmunol. **101:**137–147.
38. **Pearce, B. D., S. C. Steffensen, A. D. Paoletti, S. J. Henriksen, and M. J. Buchmeier.** 1996. Persistent dentate granule cell hyperexcitability after neonatal infection with lymphocytic choriomeningitis virus. J. Neurosci. **16:**220–228.
39. **Pearce, B. D., N. M. Valadi, C. L. Po, and A. H. Miller.** 2000. Viral infection

of developing GABAergic neurons in a model of hippocampal disinhibition. Neuroreport **11:**2433–2438.
40. **Rakic, P.** 1971. Neuron-glia relationship during granule cell migration in developing cerebellar cortex. A Golgi and electron-microscopic study in *Macaca rhesus*. J. Comp. Neurol. **141:**283–312.
41. **Seri, B., J. M. Garcia-Verdugo, B. S. McEwen, and A. Alvarez-Buylla.** 2001. Astrocytes give rise to new neurons in the adult mammalian hippocampus. J. Neurosci. **21:**7153–7160.
42. **Sheinbergas, M.** 1976. Hydrocephalus due to prenatal infection with lymphocytic choriomeningitis virus. Infection **4:**185–191.
43. **Switzer, R. C., J. de Olmos, and L. Heimer.** 1985. Olfactory system, p. 1–36. *In* G. Paxinos (ed.), The rat nervous system, vol. 1: forebrain and midbrain. Academic Press, New York, N.Y.
44. **Welsh, R. M., and M. B. A. Oldstone.** 1977. Inhibition of immunological injury of cultured cells infected with lymphocytic choriomeninigitis virus: role of defective interfering virus in regulating viral antigenic expression. J. Exp. Med. **145:**1449–1468.
45. **Wright, K. E., M. S. Salvato, and M. J. Buchmeier.** 1989. Neutralizing epitopes of lymphocytic choriomeningitis virus are conformational and require both glycosylation and disulfide bonds for expression. Virology **171:** 417–426.
46. **Wright, R., D. Johnson, M. Neumann, T. G. Ksiazek, P. Rollin, R. V. Keech, D. J. Bonthius, P. Hitchon, C. F. Grose, W. E. Bell, and J. F. Bale.** 1997. Congenital lymphocytic choriomeningitis virus syndrome: a disease that mimics congenital toxoplasmosis or cytomegalovirus infection. Pediatrics **100:**1–6. [Online.]